Self-contained solution to the spatially inhomogeneous electron Boltzmann equation in a cylindrical plasma positive column

L. L. Alves,[1] G. Gousset,[2] and C. M. Ferreira[1]
[1]*Centro de Electrodinâmica, Instituto Superior Técnico, 1096 Lisboa Codex, Portugal*
[2]*Laboratoire de Physique des Gaz et des Plasmas, Université de Paris-Sud, 91405 Orsay Cedex, France*
(Received 30 July 1996)

In this paper we develop a *self-contained formulation* to solve the steady-state spatially inhomogeneous electron Boltzmann equation (EBE) in a plasma positive column, taking into account the spatial gradient and the space-charge field terms. The problem is solved in cylindrical geometry using the classical two-term approximation, with appropriate boundary conditions for the electron velocity distribution function, especially at the tube wall. A condition for the microscopic radial flux of electrons at the wall is deduced, and a detailed analysis of some limiting situations is carried out. The present formulation is *self-contained* in the sense that the electron particle balance equation is exactly satisfied, that is, the ionization rate exactly compensates for the electron loss rate to the wall. This condition yields a relationship between the applied maintaining field and the gas pressure, termed the *discharge characteristic*, which is obtained as an *eigenvalue solution* to the problem. By solving the EBE we directly obtain the isotropic and the anisotropic components of the electron distribution function (EDF), from which we deduce the radial distributions of all relevant macroscopic quantities: electron density, electron transport parameters and rate coefficients for excitation and ionization, and electron power transfer. The results show that the values of these quantities across the discharge are lower than those calculated for a homogeneous situation, due to the loss of electrons to the wall. The solutions for the EDF reveal that, for sufficiently low maintaining fields, the radial anisotropy at some radial positions can be negative, that is, directed toward the discharge axis, for energies above a *collisional barrier* around the inelastic thresholds. However, at the wall, the radial anisotropy always points to the wall, due to the strong electron drain occuring in this region. We further present pertinent comparisons with other formulations recently proposed in the literature to model the present inhomogeneous problem. [S1063-651X(97)09901-7]

PACS number(s): 52.25.Dg, 51.10.+y, 52.25.Fi

I. INTRODUCTION

In recent years there has been increasing interest devoted to the problem of nonlocal electron kinetics in various discharge and/or discharge field configurations, due to the growing number of technological applications involving low-temperature plasmas. In fact, the spatial description of the electron kinetics is fundamental not only to further understand the physical phenomena inside a gas discharge, but also to provide practical information about the type of discharge to adopt for given applications. This motivation led to the development of various nonequilibrium discharge models and, in many cases, to the introduction of numerical tools in order to solve the problem in an efficient, accurate way.

An impressive illustration of this are the very complete *hybrid models* of rf capacitively coupled discharges (CCD's) and inductively coupled discharges (ICD's) [1–7]. In general, these *hybrid models* are assembled using different modules, each of which is designed to calculate some important physical quantity: the electron distribution function (EDF), the distribution of fields, the density profiles, and so on. The main problem with these sophisticated models is that they usually require very long computation times, particularly for the electron kinetic calculations using either *particle-in-cell and Monte Carlo* simulations [2,7,8] or a *convective scheme* to numerically integrate the Boltzmann equation [9–11].

The amount of computational work required to study the electron kinetics can greatly be reduced if the electron Boltzmann equation (EBE) is written under certain approximations, e.g., the *two-term approximation*, when the discharge anisotropies are small [12–14], and/or the *dc effective field approximation*, when the discharges are produced by hf applied electric fields [12,13,15]. Many authors have adopted such descriptions to solve the EBE using a variety of numerical techniques in order to speed up the calculations [16–18]. Other authors have solved the EBE by adopting the so-called *total energy formulation*, in which the *total energy* (kinetic plus potential) of the electrons replaces the kinetic energy as independent variable.

The *total energy formulation* has been used to work out solutions to the complete spatially inhomogeneous EBE in various situations, such as the analysis of the plasma electron response to a spatially embedded electric field impulse [19], or the radial study of the electron kinetics in a classical dc positive column [20,21]. In *weakly collisional cases*, when the electron mean free path is of the order of the typical discharge dimensions, the EBE can be written using the *total energy* of the electrons as the sole independent variable to describe the nonequilibrium electron kinetics. This approximation corresponds to the so-called *nonlocal approach*, based on the works of Bernstein and Holstein [22] and Tsendin [23], in which the EDF becomes a spatially homogeneous function to be determined from a spatially averaged kinetic equation.

The basic advantage of this approach is that it not only considerably reduces the computational labor to solve the

EBE (now transformed into a single variable equation), but further allows analytical or semianalytical solutions to be obtained in some limiting cases. As a consequence, the *nonlocal approach* has been applied to the study of a wide variety of problems in gas discharge physics, such as the classical dc positive column [24], the anode and the cathode regions of a dc glow discharge [25,26], and the modeling of low-pressure rf CCD's [27], ICD's [28–31], and surface-wave discharges [32].

The contribution of these models was decisive to construct an overall picture of the electron kinetics in inhomogeneous situations. However, the various formulations adopted so far to solve this nonlocal kinetic problem still require some improvements in order to achive a *self-contained description*.

The reasons for this are twofold. First, the nonlocal electron kinetics are strongly dependent on the phenomena occuring at the plasma-sheath boundary near the discharge wall, where the anisotropies are expected to increase. To gain further physical insight into this problem one has to derive a correct *wall boundary condition* from *theoretical considerations*, instead of assuming any arbitrary law at the wall [17,18,21]. Busch and Kortshagen [20] deduced a wall boundary condition using the *total energy formulation* along with the physical arguments previously presented by Tsendin and Golubovskii [24]. However, the *total energy formulation* demands a considerable effort of theoretical development, so that a boundary condition directly applying to the electron velocity distribution function was not derived in [20]. Second, a *self-contained steady-state solution* to the EBE must verify the electron particle balance equation. This requirement yields a relationship between the discharge maintaining field and the pressure, termed the *discharge characteristic*, which has to be *simultaneously* obtained as an *eigenvalue solution* to the problem. Such a formulation constitutes the sole correct approach for consistently solving this nonlocal kinetic problem, as it does not resort to experimental (or parametric) *discharge characteristics* as input data [20,21,33].

The purpose of this paper is to develop a *self-contained formulation* to numerically solve the spatially inhomogeneous EBE in a plasma positive column, including the spatial gradient and the space-charge field terms in the equation for the isotropic component. The problem is solved in cylindrical geometry, with appropriate boundary conditions for the electron velocity distribution function, especially at the tube wall, where a detailed discussion is carried out.

The organization of the paper is the following. In Sec. II, we develop the general formulation for the radially dependent EBE and the boundary conditions, and we discuss its validity domain *versus* the pressure. In Sec. III, we analyze some limiting cases for the wall boundary condition used in this work, and show that the results obtained in other theories are recovered. The electron particle and power balance equations are deduced in Sec. IV, by integrating the EBE in energy space. In Sec. V, we present the independent input parameters and the *eigenvalue solution* to the EBE; the numerical method employed to solve the problem is described in Sec. VI. In Sec. VII, we introduce the space-charge field profile adopted in this work, and discuss the *total energy formulation*. The results obtained are discussed in Sec. VIII, and the concluding remarks are presented in Sec. IX.

II. RADIALLY DEPENDENT ELECTRON BOLTZMANN EQUATION

A. General formulation

The system under analysis is a dc positive column of radius R, under the action of a total electric field of the form $\vec{E}(r)=E_r(r)\vec{e}_r+E_z\vec{e}_z$, where the radial component $E_r(r)=-\nabla_r\phi$ is the space-charge field (ϕ represents the space-charge potential), and the axial one is the applied electric field, assumed to be uniform. For the present discussion, involving only the study of the electron kinetics, a given radial profile for the space-charge field is assumed.

The distribution of electrons in the discharge can be described by the EDF $F(r,\vec{v})$, representing the number density of electrons at the point $(r,\vec{v})$ in phase space. The EDF is obtained by solving the corresponding Boltzmann equation with the normalization condition $\int F(r,\vec{v})d^3v=n(r)$, where $n(r)$ is the electron density.

In the present situation, we consider the existence of a total anisotropy with an axial component due to the applied field, and a radial component due to the space-charge field and the density gradient. In order to solve the EBE we adopt the well-known *small anisotropy approximation* [12,13], that is, we represent the EDF by the first two terms of its expansion in spherical harmonics around the total anisotropy direction $\vec{e}_{\text{anisotropy}}$,

$$F(r,v,\theta)=\sum_{l=0}^{\infty}F^l(r,v)P_l(\cos\theta) \tag{1a}$$

$$\simeq F^0(r,v)+F^1(r,v)\cos\theta$$

$$=F^0(r,v)+\frac{\vec{v}}{v}\cdot\vec{F}^1(r,v). \tag{1b}$$

In these equations, $P_l(\cos\theta)$ denotes the l Legendre polynomial, and $\vec{F}^1\equiv F^1\vec{e}_{\text{anisotropy}}$ is the *first-anisotropy vector*.

With this approximation, the EDF is decoupled into an isotropic component $F^0(r,v)$, an axial anisotropic component $F_z^1(r,v)$, and a radial anisotropic component $F_r^1(r,v)$. Introducing expansion (1b) into the EBE yields a scalar equation for the isotropic component of the EDF, and a two-fold vector equation for its anisotropic components. After the renormalization,

$$\frac{F^0(r,v)}{n_0}4\pi v^2dv\equiv f(r,u)\sqrt{u}du,$$

$$\frac{F^1(r,v)}{n_0}4\pi v^2dv\equiv f^1(r,u)\sqrt{u}du,$$

where n_0 is the electron density at the tube axis, so that

$$\int_0^{\infty}f(r,u)\sqrt{u}du=\frac{n(r)}{n_0}\Rightarrow\int_0^{\infty}f(0,u)\sqrt{u}du=1, \tag{2}$$

one obtains [12,13]

$$\frac{\partial G(r,u)}{\partial u}+\left(\frac{2e}{m}\right)^{1/2}\frac{u}{3}\vec{\nabla}_r\cdot\vec{f}^1(r,u)\simeq\sqrt{u}[J(r,u)+I(r,u)], \tag{3a}$$

$$f_z^1(r,u)\simeq\frac{1}{N\sigma_t(u)}E_z\frac{\partial f(r,u)}{\partial u}, \tag{3b}$$

$$f_r^1(r,u)\simeq\frac{1}{N\sigma_t(u)}\left[E_r(r)\frac{\partial f(r,u)}{\partial u}-\nabla_r f(r,u)\right]. \tag{3c}$$

Herein, $G=G_E+G_c$ is the *total upflux* in energy space due to the total field and the elastic collisions given by, respectively,

$$G_E(r,u)\equiv G_{E_z}(r,u)+G_{E_r}(r,u)$$
$$\equiv-\left(\frac{2e}{m}\right)^{1/2}\frac{u}{3}[E_z f_z^1(r,u)+E_r(r)f_r^1(r,u)], \tag{4a}$$

$$G_c(r,u)\equiv-\left(\frac{2e}{m}\right)^{1/2}\frac{2m}{M+m}Nu^2\sigma_c(u)$$
$$\times\left[f(r,u)+\frac{k_BT_g}{e}\frac{\partial f(r,u)}{\partial u}\right]. \tag{4b}$$

In these equations, $u=mv^2/2e$ is the electron energy in eV, where e and m are the electron charge and mass, respectively; M is the atom mass; N is the gas density; T_g is the gas temperature; $\sigma_t(u)=\sigma_c(u)+\Sigma_i\sigma_0^i(u)+\sigma_0^I(u)$ is the total electron-neutral momentum transfer cross section; $\sigma_c(u)$ is the elastic momentum transfer cross section; $\sigma_0^i(u)$ is the direct electron excitation cross section for the ith state; and $\sigma_0^I(u)$ is the direct electron ionization cross section (all inelastic collisional processes are assumed to be isotropic). The quantities $J(r,u)$ and $I(r,u)$ represent electron operators for the collisional processes here considered, i.e., ground state excitations and ionization, taking into account the production of secondary electrons, respectively:

$$J(r,u)\equiv\left(\frac{2e}{m}\right)^{1/2}\frac{N}{\sqrt{u}}\sum_i[(u+V_i)\sigma_0^i(u+V_i)f(r,u+V_i)$$
$$-u\sigma_0^i(u)f(r,u)], \tag{5a}$$

$$I(r,u)\equiv\left(\frac{2e}{m}\right)^{1/2}\frac{N}{\sqrt{u}}\left[\int_{2u+V_I}^{\infty}u'\sigma_I^{\rm sec}(u',u)f(r,u')du'\right.$$
$$+\int_{u+V_I}^{2u+V_I}u'\sigma_I^{\rm sec}(u',u'-V_I-u)f(r,u')du'$$
$$\left.-u\sigma_0^I(u)f(r,u)\right]. \tag{5b}$$

In these equations, V_i and V_I are the energy of the ith state and the ionization state, respectively, and $\sigma_I^{\rm sec}(u',u)$ is the differential direct ionization cross section for the production of a secondary electron of energy u from the collision of a ground-state atom with a primary electron of energy u'. This differential cross section verifies the integral relation

$$\sigma_0^I(u)=\int_0^{(u-V_I)/2}\sigma_I^{\rm sec}(u,u')du'. \tag{6}$$

Equations (3b) and (3c) determine the anisotropic components $f_z^1(r,u)$ and $f_r^1(r,u)$ as a function of the isotropic component $f(r,u)$.

The first term on the left-hand side of Eq. (3a) represents the divergence of the electron flux in energy space driven by the applied field, the space-charge field, and the recoil collisions, respectively, while the second term represents the divergence of the electron flux in configuration space. The terms on the right-hand side of Eq. (3a) represent the net creation rate of electrons with a given energy due to the excitation and ionization processes, respectively. Substituting Eqs. (3b), (3c), (4a), and (4b) into Eq. (3a) yields a second-order partial differential equation (PDE) for $f(r,u)$, in the energy and configuration spaces; this equation is to be solved subject to appropriate boundary conditions.

B. Validity domain versus pressure

For the purpose of analyzing the validity domain of the EBE with the pressure, we will use estimations based on simple orders of magnitude. The basic question here is to know the applicability conditions of the *small anisotropy approximation* according to the range of pressures considered.

In view of this, let us focus on Eqs. (3b) and (3c) for the EDF anisotropic components. For the purposes of estimation, we note that $1/(N\sigma_t)=\lambda$ (λ is the electron mean free path), $\partial f/\partial u\sim -f/\langle u\rangle$ ($\langle u\rangle$ represents the mean energy of the electrons), and $\nabla_r f\sim -f/R$, so that

$$f_z^1\simeq-\frac{E_z\lambda}{\langle u\rangle}f, \tag{7a}$$

$$f_r^1\simeq\left[-\frac{E_r\lambda}{\langle u\rangle}+\frac{\lambda}{R}\right]f. \tag{7b}$$

From Eq. (7a), we conclude that the axial anisotropy can be kept small provided $E_z\lambda\ll\langle u\rangle$, which means that the energy gained from the applied electric field between two successive collisions, $E_z\lambda$, must be much smaller than the mean energy of the electrons [34].

The limitation of the radial anisotropy, however, further requires that the two terms on the right-hand side of Eq. (7b) must be of the same order of magnitude, i.e., $E_r\lambda/\langle u\rangle\simeq\lambda/R$, or equivalently $\lambda/R\ll E_r/E_z$. The fulfillment of this latter condition strongly depends on pressure, and may be difficult to meet: at low pressures ($\lambda\gtrsim R$) it requires the space-charge field to be higher than the applied maintaining field ($E_r>E_z$), which is certainly not the case near the discharge axis; at high pressures ($\lambda\ll R$) it requires that the applied maintaining field dominates over the space-charge field ($E_z\gg E_r$), a condition that may be violated near the wall. The situations here considered are limited to a range of intermediate to high pressures, where collisional

processes play an important role in the electron kinetics and $E_z > E_r$ across most of the discharge radius (see Sec. VII).

C. Boundary conditions

The solution of Eq. (3a) requires the knowledge of two boundary conditions in energy space and two boundary conditions in configuration space. In energy space we impose [13]

$$G(r,0)=G(r,\infty)=0, \tag{8}$$

corresponding to the *total upflux* conservation

$$\int_0^\infty \frac{\partial G(r,u)}{\partial u}\,du = G(r,\infty)-G(r,0)\equiv 0,$$

whereas in configuration space, at $r=0$, symmetry considerations lead to

$$\left.\frac{\partial f(r,u)}{\partial r}\right|_{r=0}=0. \tag{9}$$

In order to deduce a *meaningful* physical boundary condition at $r=R$, we first obtain the *net* (*microscopic*) *flux of electrons with velocity between* v *and* $v+dv$, $\vec{\gamma}(r,v)$, by integrating the product $F(r,\vec{v})\vec{v}$ over all angles in velocity space,

$$\vec{\gamma}(r,v)\equiv \int\int_\Omega F(r,\vec{v})\vec{v}\,d\Omega. \tag{10}$$

Substituting the *full expansion* (1a) into Eq. (10), and taking into account the orthonormality properties of the Legendre polynomials [35], yields

$$\vec{\gamma}(r,v)=\frac{4\pi v}{3}F^1(r,v)\vec{e}_{\text{anisotropy}}. \tag{11}$$

As expected, the $\vec{\gamma}$ flux has the same direction as the total anisotropy, its components being given by

$$\vec{\gamma}(r,v)=\vec{\gamma}_r(r,v)+\vec{\gamma}_z(r,v), \tag{12a}$$

$$\vec{\gamma}_r(r,v)=\frac{4\pi v}{3}F_r^1(r,v)\vec{e}_r, \tag{12b}$$

$$\vec{\gamma}_z(r,v)=\frac{4\pi v}{3}F_z^1(r,v)\vec{e}_z. \tag{12c}$$

It is clear that the wall boundary condition must be derived from the continuity of $\vec{\gamma}_r$ at $r=R$, taking into account that some electrons are reflected by the (space-charge) potential barrier and, thus, do not reach the wall. The mathematical formulation of this basic idea is, however, somewhat difficult to carry out, due to the nature of the different physical processes influencing the electron motion toward the wall, as the collisional scattering, the drift under the action of the total field, and the sink of electrons due to collisions with the wall.

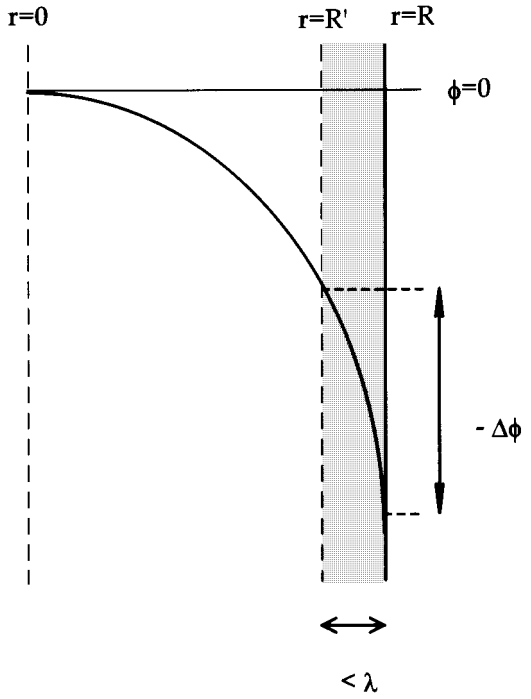

FIG. 1. Schematic diagram of the potential drop $\Delta\phi$, across the noncollisional *boundary layer* $R'<r<R$ ($R-R'\lesssim\lambda$ and λ is the electron mean free path). The discharge axis is at $r=0$ and the discharge wall is at $r=R$.

A solution to this problem can be sought through a separation of these processes. To this end, let us first note that electron collisions do not occur within a wall *boundary layer* with a thickness of the order of the electron mean free path ($R'\leqslant r\leqslant R$ and $R-R'\lesssim\lambda$). In this region, no electrons are created, and the space-charge field is expected to dominate over the applied field, so that a Boltzmann distribution law can be assumed for the electron density.

This collisionless *boundary layer* is not to be identified with the wall space-charge sheath, as collisions can occur in the latter for the range of pressures studied in this work. Within the collisionless *boundary layer* the electron kinetics can be described in terms of energy conservation only, as the motion is determined exclusively by the space-charge potential drop $\Delta\phi$ (see Fig. 1).

It is also important to note that the EBE, as given by Eqs. (3a)–(4b), has no physical meaning (and consequently *no validity*) inside the above *boundary layer*, since the derivation of the EBE is based on a *coarse graining* procedure over a length scale much greater than the mean free path [36,37]. Therefore, Eqs. (3a)–(4b) are only valid across the tube up to the *boundary layer* position ($0\leqslant r\leqslant R'$).

In order to deduce the wall boundary condition, we must determine which electrons can overcome the potential drop $\Delta\phi$. For this purpose it is convenient to decompose the electron velocity $\vec{v}$ as (see Fig. 2)

$$\vec{v}=v_\perp\vec{e}_\perp+v_\parallel\vec{e}_\parallel=v\cos\chi\vec{e}_\perp+v\sin\chi\vec{e}_\parallel,$$

where $\vec{e}_\perp\equiv\vec{e}_r$ and $\vec{e}_\parallel$ are, respectively, the perpendicular and the parallel unit vectors to the discharge boundary, assuming planar geometry for simplicity. Similarly, the electron kinetic energy can be decomposed as

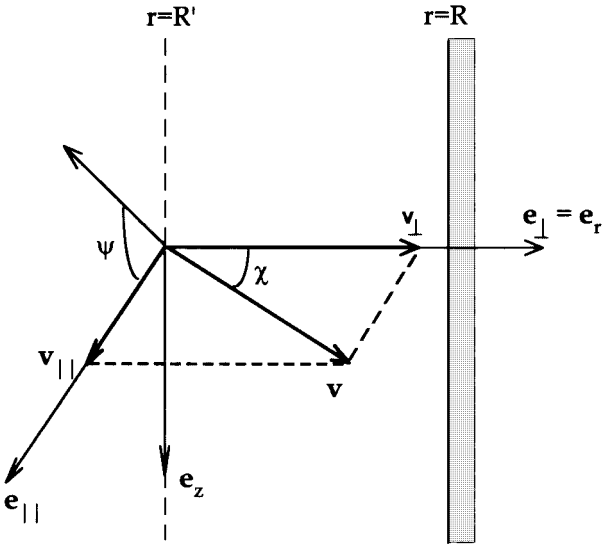

FIG. 2. Electron velocity decomposition in the *boundary layer* $R'<r<R$.

$$u=\frac{1}{2}\frac{mv^2}{e}=\frac{1}{2}\frac{m(v_\perp^2+v_\parallel^2)}{e}=u_\perp+u_\parallel,$$

where

$$u_\perp=\frac{1}{2}\frac{mv_\perp^2}{e}=\frac{1}{2}\frac{mv^2}{e}\cos^2\chi=u\cos^2\chi, \tag{13a}$$

$$u_\parallel=\frac{1}{2}\frac{mv_\parallel^2}{e}=\frac{1}{2}\frac{mv^2}{e}\sin^2\chi=u\sin^2\chi. \tag{13b}$$

In order to be able to cross the *boundary layer*, from R' to R, an electron must have a kinetic energy along r, $u_\perp$, greater than the potential drop $\Delta\phi$, that is,

$$u_\perp\geqslant\Delta\phi\Rightarrow\cos^2\chi\geqslant\frac{\Delta\phi}{u}\equiv\cos^2\chi^\star$$

$$\Rightarrow\chi\leqslant\chi^\star(u)=\arccos\left(\frac{\Delta\phi}{u}\right)^{1/2}. \tag{14}$$

Consequently, one can define a *loss cone to the wall* [24] corresponding to the solid angle (see Fig. 3)

$$\Delta\Omega^\star(u)\equiv\int\int_{\Omega^\star(u)}d\Omega^\star=\int_{\psi=0}^{\psi=2\pi}\int_{\chi=0}^{\chi=\chi^\star(u)}\sin\chi\,d\chi\,d\psi$$

$$=2\pi(1-\cos\chi^\star(u)), \tag{15}$$

where $\chi^\star(u)$, representing the maximum polar angle for a given energy u, is defined by the set of conditions

$$\chi^\star(u)=\begin{cases}0 & \text{if } u_\perp\leqslant u\leqslant\Delta\phi\\ \arccos\left(\dfrac{\Delta\phi}{u}\right)^{1/2} & \text{if } u\geqslant u_\perp\geqslant\Delta\phi.\end{cases} \tag{16}$$

The γ_r flux conservation in the *boundary layer* can be expressed by the condition

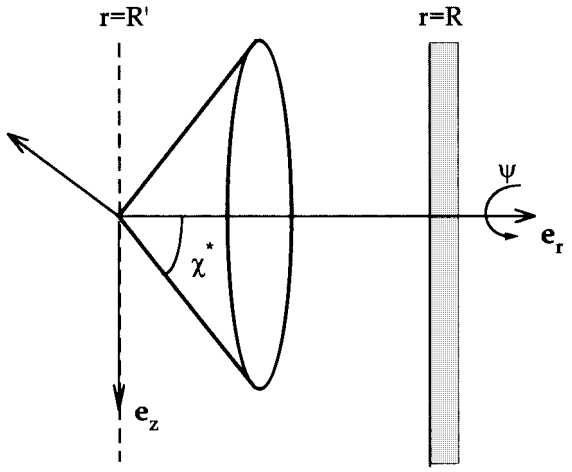

FIG. 3. The *loss cone* to the wall. The quantity $\chi^\star$ represents the maximum polar angle for which the kinetic energy along r, $u_\perp$, is still greater than the potential drop $\Delta\phi$.

$$\gamma_r(R,v)=\gamma_r^+(R',v)-\gamma_r^-(R',v), \tag{17}$$

where $\gamma_r^+(R',v)$ $[\gamma_r^-(R',v)]$ is the *forward* (*backward*) *microscopic radial electron flux at* $r=R'$, that is, the total number of electrons, with velocity between v and $v+dv$, entering (leaving) the *boundary layer* per unit area and unit time.

In general, $\gamma_r^-(R',v)$ is defined as

$$\gamma_r^-(R',v)\equiv\zeta\gamma_r^+(R',v), \tag{18}$$

where ζ is the wall reflection coefficient ($\zeta=0$ corresponds to a perfectly absorbing wall), while $\gamma_r^+(R',v)$ is given by (see Fig. 3)

$$\gamma_r^+(R',v)=\int\int_{\Omega^\star}F(R',\vec{v})v_r\,d\Omega^\star$$

$$=\int_{\psi=0}^{\psi=2\pi}\int_{\chi=0}^{\chi=\chi^\star(v)}F(R',\vec{v})(v\cos\chi)\sin\chi\,d\chi\,d\psi. \tag{19}$$

If we now assume that the EDF can be well represented by the two-term expansion in spherical harmonics (1b), we can solve the integrals in Eq. (19), yielding

$$\gamma_r^+(R',v)=\int_{\psi=0}^{\psi=2\pi}\int_{\chi=0}^{\chi=\chi^\star(v)}\left[F^0(R',v)+\frac{\vec{v}}{v}\cdot\vec{F}^1(R',v)\right]$$

$$\times(v\cos\chi)\sin\chi\,d\chi\,d\psi$$

$$=2\pi v\left[\frac{1-\cos^2\chi^\star(v)}{2}F^0(R',v)\right.$$

$$\left.+\frac{1-\cos^3\chi^\star(v)}{3}F_r^1(R',v)\right]. \tag{20}$$

The situations considered in the present work are limited to a range of intermediate to high pressures (cf. Sec. II B), such that the electron mean free path is much smaller than the typical discharge dimension ($\lambda\ll R$). Thus, an *infinitely thin boundary layer* can be assumed.

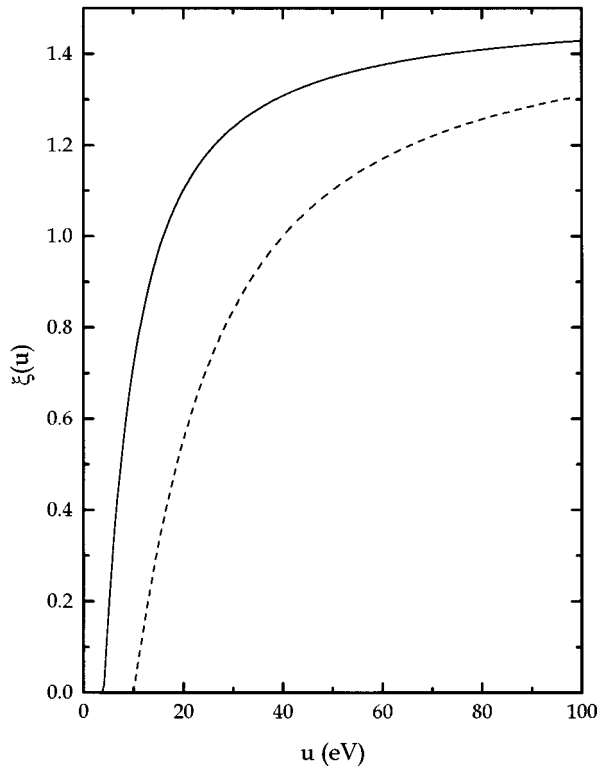

FIG. 4. The ξ factor for the wall boundary condition. The curves were calculated for the following potential drops $\Delta\phi$: solid curve, 4 V; dashed curve, 10 V.

The final form of the wall boundary condition is now readily obtained from Eqs. (12b), (17), (18), and (20) (with $R' \to R$), yielding

$$f_r^1(R,u) = \xi(u) f(R,u), \tag{21a}$$

$$\xi(u) = \frac{3}{2\left(\frac{1+\zeta}{1-\zeta}\right) + \cos^3\chi^\star(u)} \quad \frac{1-\cos^2\chi^\star(u)}{}, \tag{21b}$$

where the usual renormalization has been used (cf. Sec. II A). Figure 4 represents ξ vs u for $\Delta\phi = 4$ V and 10 V.

For the purpose of calculations we have assumed a *perfectly absorbing wall*, so we can write [cf. Eqs. (16) and (21b)]

$$\xi(u) = \begin{cases} 0 & \text{if } u \leqslant \Delta\phi \\ \dfrac{3}{2}\dfrac{1-(\Delta\phi/u)}{1+(\Delta\phi/u)^{3/2}} & \text{if } u \geqslant \Delta\phi. \end{cases} \tag{22}$$

Note that the wall boundary condition given by Eqs. (21a) and (22) implies that $f_r^1 > 0$ for $u \geqslant \Delta\phi$, which means that the radial anisotropy always points toward the wall at $r = R$.

The introduction of a *loss cone to the wall* in order to deduce a boundary condition for the electrons has previously been used by other authors [20,24]. These authors, however, did not formally associate this concept with the microscopic electron flux (11), so the boundary conditions they derived are not directly expressed in terms of the f_r^1 anisotropy. The advantage of the present formulation is that it gives a direct control upon the electron transport features.

III. LIMITING CASES FOR THE WALL BOUNDARY CONDITION

In this section we will analyze some limits of the wall boundary condition deduced in Sec. II C, in order to show that it reproduces the results obtained from other theories.

A. Free diffusion approximation

The *free diffusion approximation* assumes that there is no potential barrier reflecting the electrons at the wall, which means that the *loss cone* sweeps all polar angles in the interval $0 \leqslant \chi \leqslant \pi/2$ ($\chi^\star = \pi/2$). In this case the equation for the γ_r flux conservation at $r = R$ writes, assuming a perfectly absorbing wall [cf. Eqs. (17) and (20)],

$$\gamma_r(R,v) = \gamma_r^+(R,v) = 2\pi v[\tfrac{1}{2} F^0(R,v) + \tfrac{1}{3} F_r^1(R,v)]. \tag{23}$$

The integration of Eq. (23) over all velocities yields

$$\Gamma_r(R) = \tfrac{1}{4} n(R)\langle v\rangle(R) + \tfrac{1}{2} n(R) v_d(R), \tag{24}$$

where

$$\Gamma_r(r) \equiv \int_0^\infty \gamma_r(r,v) v^2 dv \tag{25}$$

is the macroscopic radial flux, and the mean velocity $\langle v\rangle$ and the radial drift velocity v_d are given by, respectively,

$$n(r)\langle v\rangle(r) = \int_0^\infty v F^0(r,v) 4\pi v^2 dv, \tag{26a}$$

$$n(r) v_d(r) = \int_0^\infty v F_r^1(r,v) \frac{4\pi v^2}{3} dv = \Gamma_r(r). \tag{26b}$$

Equation (24), a well-known expression obtained in the framework of the *free diffusion approximation* [38,39], can be combined with Eq. (26b) to give

$$v_d(R) = \frac{1}{2}\langle v\rangle(R), \tag{27}$$

which constitutes a widely used macroscopic boundary condition at an absorbing surface for the diffusion of electrons in a scattering medium [40–44].

By using expression (12b) for the γ_r flux, we can rewrite Eq. (23), after energy renormalization, as

$$f_r^1(R,u) = \tfrac{3}{2} f(R,u). \tag{28}$$

Equation (28), the asymptotic limit of Eqs. (21a) and (21b) for $\chi^\star = \pi/2$ and $\zeta = 0$, is currently used in photon diffusion theory [45] and neutron diffusion theory [46], where no interactions with electric fields exist. Although condition (28) implies a clear violation of the *small anisotropy approximation*, it has nevertheless been widely used in the literature

as it ''gives a better approximation to the exact solution than we should have the right to expect'' [45].

B. Two-stream approximation—Milne's boundary condition

The *two-stream approximation* was used by several authors [47–50] to solve the transport equations of uncharged particles diffusing in an isotropic scattering medium. This approach consists in replacing the angular distribution of scattered particles with a pair of representative *monokinetic streams*, one with intensity I_+ moving at angle θ_I to the $\vec{e}_{\text{anisotropy}}$ direction, and the other with intensity I_- moving at angle θ_I to the $-\vec{e}_{\text{anisotropy}}$ direction. Scattering from I_+ results in particles that remain in I_+ or that join the I_- stream. The reader should refer to [51–53] for a detailed discussion of the formulation.

By applying this approximation to the transport of electrons, assuming $E_r(r)=0$ and $\vec{e}_{\text{anisotropy}} \simeq \vec{e}_r$, the net microscopic radial flux at the wall, $\gamma_r(R,v)$, is written [cf. Eqs. (10) and (11)]

$$\begin{aligned}\gamma_r(R,v) &= 2\pi \int_0^{\pi} F(R,v,\theta) v_r \sin\theta \, d\theta \\ &\simeq 2\pi F_r^1(R,v)\cos\theta_I (v\cos\theta_I) \int_0^{\pi} \sin\theta \, d\theta \\ &= 4\pi v F_r^1(R,v)\cos^2\theta_I , \end{aligned} \tag{29}$$

and the forward microscopic radial flux at the wall, $\gamma_r^+(R,v)$, becomes [cf. Eqs. (19) and (20)]

$$\begin{aligned}\gamma_r^+(R,v) &= 2\pi \int_0^{\pi/2} F(R,v,\theta) v_r \sin\theta \, d\theta \\ &\simeq 2\pi F^0(R,v)(v\cos\theta_I) \int_0^{\pi/2} \sin\theta \, d\theta \\ &\quad + 2\pi F_r^1(R,v)\cos\theta_I (v\cos\theta_I) \int_0^{\pi/2} \sin\theta \, d\theta \\ &= 2\pi v [F^0(R,v)\cos\theta_I + F_r^1(R,v)\cos^2\theta_I]. \end{aligned} \tag{30}$$

The radial flux conservation at $r=R$ is obtained from Eqs. (17) and (18) using Eqs. (29) and (30) (assuming $R' \simeq R$ and adopting the usual renormalization), which yields

$$f_r^1(R,u) = \frac{1}{\cos\theta_I} \frac{1-\zeta}{1+\zeta} f(R,u), \tag{31}$$

where the radial anisotropy is now given by [cf. Eq. (3c)]

$$f_r^1(R,u) = -\frac{1}{N\sigma_t(u)} \nabla_r f(r,u)|_{r=R}. \tag{32}$$

The integration of Eqs. (31) and (32) over the energy space yields

$$\left| \frac{\nabla_r n(r)}{n(r)} \right|_{r=R} = \frac{N\sigma_t}{\cos\theta_I} \frac{1-\zeta}{1+\zeta}, \tag{33}$$

where we have used the fact that the electron streams are monokinetic, together with the normalization condition (2) for the EDF.

If we now adopt a Gaussian weight factor of $\cos\theta_I = 1/\sqrt{3}$ as discussed by Chandrasekhar [50], and note that the mean electron collisional mean free path is $\lambda = 1/(N\sigma_t)$, Eq. (33) assumes the familiar form of the *Milne's boundary condition* for the magnitude of the normalized electron density slope at $r=R$ [46,51–54],

$$\left| \frac{\nabla_r n(r)}{n(r)} \right|_{r=R} = \frac{\sqrt{3}}{\lambda} \frac{1-\zeta}{1+\zeta}. \tag{34}$$

C. Ambipolar diffusion approximation

The classical *ambipolar diffusion approximation* assumes a vanishing electron density at the wall, which amounts to assuming an infinite potential barrier at the wall reflecting *all* the electrons, that is,

$$\begin{aligned}&\Delta\phi \to -\infty \Rightarrow \chi^{\star}(u) \to 0 \Rightarrow \xi(u) = 0 \Rightarrow f_r^1(R,u) \\ &\quad = \frac{1}{N\sigma_t(u)} \left[E_r(R) \frac{\partial f(R,u)}{\partial u} - \nabla_r f(R,u) \right] = 0. \end{aligned} \tag{35}$$

Equation (35) can be solved analytically using separation of variables, to yield the well-known Maxwell-Boltzmann distribution

$$f(R,u) = A\exp[-\alpha(u-\phi(R))] \to 0,$$

which vanishes at $r=R$ due to the space-charge potential singularity. The usual wall boundary condition for the electron density in the ambipolar diffusion limit, $n(R)/n_0 = \int_0^{\infty} f(R,u)\sqrt{u}\,du = 0$ [55,56], is therefore recovered by the present formulation.

IV. INTEGRATION OF THE EBE—MACROSCOPIC EQUATIONS

A. Electron particle balance equation

The electron particle balance equation is obtained by integrating Eq. (3a) over all energies, taking into account the boundary conditions in energy space, Eq. (8). The resulting equation is

$$\frac{1}{3}\left(\frac{2e}{m}\right)^{1/2} \vec{\nabla}_r \cdot \int_0^{\infty} \vec{f}_r^1(r,u) u\,du = \nu_I(r) \frac{n(r)}{n_0}, \tag{36}$$

where $\nu_I(r)$ is the direct ionization collision frequency given by the expression [$\nu_I(r)/N$ is the corresponding rate coefficient]

$$\frac{\nu_I(r)}{N} \frac{n(r)}{n_0} = \left(\frac{2e}{m}\right)^{1/2} \int_0^{\infty} \sigma_0^I(u) f(r,u) u\,du. \tag{37}$$

The left-hand side of Eq. (36) is just the divergence of the reduced radial flux Γ_r/n_0, which can be obtained by integrating Eq. (3c) over all energies. This yields [cf. Eq. (26b)]

$$\frac{\Gamma_r(r)}{n_0}=\frac{1}{n_0}\int_0^\infty F_r^1(r,v)\frac{4\pi v^3}{3}dv=\frac{1}{3}\left(\frac{2e}{m}\right)^{1/2}\int_0^\infty f_r^1(r,u)u\,du$$

$$=-\nabla_r\left(D(r)\frac{n(r)}{n_0}\right)-\mu(r)\frac{n(r)}{n_0}E_r(r), \tag{38}$$

where $D(r)$ and $\mu(r)$ are the electron free diffusion coefficient and the electron mobility, respectively, given by

$$D(r)N\frac{n(r)}{n_0}=\frac{1}{3}\left(\frac{2e}{m}\right)^{1/2}\int_0^\infty\frac{u}{\sigma_t(u)}f(r,u)du, \tag{39a}$$

$$\mu(r)N\frac{n(r)}{n_0}=-\frac{1}{3}\left(\frac{2e}{m}\right)^{1/2}\int_0^\infty\frac{u}{\sigma_t(u)}\frac{\partial f(r,u)}{\partial u}du. \tag{39b}$$

Therefore, Eq. (36) corresponds to the electron continuity equation, expressing the equality between the rates for electron creation and loss in the discharge

$$\vec{\nabla}_r\cdot\vec{\Gamma}_r(r)=\nu_I(r)n(r). \tag{40}$$

Up to now, most of the kinetic modeling of active plasmas using the EBE has been based on the *homogeneous* (space-independent) assumption, neglecting altogether, for consistency, the loss of electrons to the wall and the production of new electrons by ionization. In this approximation, and for the purposes of discharge modeling, one must take into account the electron continuity equation *independently* of the Boltzmann equation, since the former is no longer implicit in the latter.

In the present situation, the solutions $f(r,u)$ to the isotropic EBE must also implicitly verify Eq. (40). Detailed information on how to solve this problem will be given later, in Secs. V and VI B.

B. Electron power balance equation

The electron power balance equation is obtained by multiplying Eq. (3a) by the electron energy u, and then integrating over all energies [taking into account the boundary conditions in energy space (8)]. The resulting equation can be written as [see also Eqs. (4a) and (4b)]

$$\Theta(r)\equiv\Theta_{\text{transp}}(r)+\Theta_{\text{coll}}(r), \tag{41}$$

with

$$\Theta_{\text{transp}}(r)\equiv P_{E_r}(r)+P_{\text{conv}}(r), \tag{42a}$$

$$\Theta_{\text{coll}}(r)\equiv P_{\text{el}}(r)+P_{\text{exc}}(r)+P_{\text{ion}}(r). \tag{42b}$$

The left-hand-side term of Eq. (41) represents the mean power absorbed from the applied field per electron, and is given by

$$\Theta(r)\frac{n(r)}{n_0}\equiv\int_0^\infty G_{E_z}(r,u)du=-\frac{\Gamma_z(r)}{n_0}E_z$$

$$=-\frac{E_z^2}{3N}\left(\frac{2e}{m}\right)^{1/2}\int_0^\infty\frac{u}{\sigma_t(u)}\frac{\partial f(r,u)}{\partial u}, \tag{43}$$

while the right-hand-side terms represent the power lost by the electrons due to the radial transport in the discharge, Θ_{transp}, and collisional processes, Θ_{coll}.

According to Eqs. (42a) and (42b), the quantity Θ_{transp} includes the power lost in flowing against the space-charge field, P_{E_r}, and the net power lost due to convection in configuration space, P_{conv}, whereas Θ_{coll} accounts for the power lost in elastic collisions, P_{el}, excitation, P_{exc}, and ionization, P_{ion}.

The explicit expressions for these terms can be written as

$$P_{E_r}(r)\frac{n(r)}{n_0}\equiv-\int_0^\infty G_{E_r}(r,u)du=\frac{\Gamma_r(r)}{n_0}E_r(r), \tag{44a}$$

$$P_{\text{conv}}(r)\frac{n(r)}{n_0}\equiv\frac{1}{3}\left(\frac{2e}{m}\right)^{1/2}\vec{\nabla}_r\cdot\int_0^\infty\vec{f}_r^1(r,u)u^2du, \tag{44b}$$

$$P_{\text{el}}(r)\frac{n(r)}{n_0}\equiv-\int_0^\infty G_c(r,u)du$$

$$=\left(\frac{2e}{m}\right)^{1/2}\frac{2m}{M+m}N\int_0^\infty u^2\sigma_c(u)$$

$$\times\left[f(r,u)+\frac{k_BT_g}{e}\frac{\partial f(r,u)}{\partial u}\right]du, \tag{44c}$$

$$P_{\text{exc}}(r)\frac{n(r)}{n_0}\equiv-\int_0^\infty J(r,u)u^{3/2}du=\sum_i V_i\nu_0^i(r)\frac{n_e(r)}{n_0}, \tag{44d}$$

$$P_{\text{ion}}(r)\frac{n(r)}{n_0}\equiv-\int_0^\infty I(r,u)u^{3/2}du=V_I\nu_0^I(r)\frac{n_e(r)}{n_0}. \tag{44e}$$

V. NORMALIZED VARIABLES. INPUT PARAMETERS AND EIGENVALUE SOLUTION

The present study involves the solution to the system formed of the EBE (3a)–(4b), with the normalization condition (2) and the boundary conditions (8), (9), (21a), and (21b). These equations are to be solved for a given gas, i.e., for a specific set of cross sections, and for appropriate values of the independent parameters involved.

By simple inspection of the above equations, it can be concluded that the proper independent parameters are E_z/N, $E_r(r)/N$ (termed the *reduced fields*), NR, and T_g, while r/R is to be taken as the independent space variable. Further, as stated in Sec. IV A, a *self-contained solution* to the isotropic EBE (3a) must verify the electron continuity equation (40); that is, it must give an ionization rate that exactly compensates for the loss rate to the wall. Assuming that $E_r(r)/N$ is known *ab initio*, this condition yields a relationship of E_z/N vs NR, termed the *discharge characteristic* for the maintaining field, which has to be *simultaneously* obtained as an *eigenvalue solution* to the problem.

Such a formulation constitutes the sole correct approach for consistently solving this nonlocal kinetic problem, as it

does not resort to experimental *discharge characteristics* as input data [20,21,33]. Of course, the problem of the determination of $E_r(r)/N$ remains open, as it can only be consistently solved by further considering the ion dynamics and Poisson's equation. This, however, is out of the scope of the present paper.

VI. NUMERICAL RESOLUTION

The numerical method employed to solve Eq. (3a) [after substitution of Eqs. (3b)–(4b)], with the boundary conditions (8), (9), (21a), and (21b), is based on its conversion into a set of N_T-coupled algebraic equations by second-order fixed-step finite differencing in both the energy and the configuration space.

This procedure (an extension of the discretization method presented in the works by Rockwood [57] and Elliot and Greene [58]) transforms the integration domain into a two-dimensional (2D) grid, where the energy axis (0 eV $<u<100$ eV) and the radial position axis ($0<r/R<1$) are divided into N_e and N_s cells, respectively. The total number of grid points is, therefore, given by $N_T=(N_e+1)\times(N_s+1)$.

Typical working values for the number of cells are $N_e=128$ and $N_s=64$, which leads to a 2D grid with $N_T=8385$ points, corresponding to a 8385×8385 dimension for the system matrix. When dealing with such matrix dimensions, direct solution techniques are immediately excluded, the option lying in iterative relaxation methods. Classical relaxation methods as, for example, the *blockwise Gauss-Seidel* one, are not suitable because of the low convergence rates (the typical order of iterations for convergence is between $N_T \ln N_T$ and N_T^2). Although computer performances have enormously increased during the last years, numerical tools are still required to efficiently solve such a large system of coupled equations.

A fast iterative technique used nowadays to solve large elliptic problems with boundary conditions is the *multigrid method* [59–61]. The great advantage of this technique is that its convergence rate does not deteriorate if the discretization step is reduced, since the typical order of iterations for convergence is N_T.

A. Multigrid method

The key idea of the *multigrid method* is that the PDE to be solved can be discretized into a sequence of 2D grids having increasingly larger cells. The calculation scheme starts at the finest grid, where some *initial solution function* is given, and it continues from one grid to another, down to the coarsest grid, and back again. On each grid a *correction function* is calculated in order to minimize the PDE error, written on the previous grid. This is made by using this correction function to appropriately modify the PDE current solution on the previous grid. The recursive repetition of this procedure throughout all grids will end with a correction of the solution function, on the finest grid.

The success of the method comes from the combination of two ideas:

(i) Smooth functions are well discretized in coarse grids.

(ii) Classical relaxation techniques considerably reduce the amplitude of the high-frequency components of the solution function error. In other words, these techniques can be used as *smoothing operators* for the function errors.

In view of this, we must perform some relaxation iterations for the PDE on each grid, in order to obtain a smooth function error whose correction will involve calculations in the next (coarser) grid.

To construct a *multigrid algorithm*, one must then choose a good smoothing method, as well as some appropriate *restriction* and *prolongation* operators, ruling the passage between grids. In this work, we have adopted alternate u-line and r-line *blockwise Gauss-Seidel* iterations as a smoothing method, together with the *nine-points prolongation* and *restriction* operators [59], in a 3-4 grid system. Another important question concerns the inclusion of boundary conditions in the *multigrid scheme*. In the algorithm here developed, at each iteration:

(i) Equations (8), (9), (21a), and (21b) are *exactly verified* on the finest grid, that is, the exact physical boundary conditions are imposed in both the energy and the configuration space.

(ii) Dirichlet boundary conditions are used in all other (coarser) grids, corresponding to a zero-error solution function at the boundaries.

The *multigrid method* was already used by other authors to solve the EBE in quite different situations [17,20], but always adopting either Dirichlet or Neumann boundary conditions. That is why the algorithm proposed in this work contains some innovative aspects, as it treats mixed, i.e., Dirichlet and Neumann, boundary conditions and it allows an *eigenvalue* calculation (see Sec. VI B). In summary, this algorithm constitutes a powerful tool for the solution of the EBE in real discharges.

B. Solution method

After discretization in both the energy and the configuration space the EBE assumes the general matrix form $\Sigma_{j=1}^{N_T} C_{ij} f_j = 0$, which shows that the EBE is a homogeneous differential equation, i.e., its right-hand side is equal to zero. As a consequence, the EBE is satisfied by an infinite set of functions, meaning that a supplementary condition must be given in order to determine a unique physical solution. This is why the EBE must be solved together with a normalization condition for $f(r,u)$.

Furthermore, we saw in Sec. V that a *self-contained solution* to the isotropic EBE (3a) yields the *discharge characteristic* for the maintaining field, E_z/N vs NR, which has to be simultaneously obtained as an *eigenvalue solution* to the problem. If E_z/N is taken as an input parameter, then the quantity NR becomes the *eigenvalue* to be determined.

In this work, the system formed by the EBE (3a)–(4b), with the boundary conditions (8), (9), (21a), and (21b), is iteratively solved using a *multigrid method*; after each iteration the solution $f(r,u)$ and the *eigenvalue* NR are modified in order to verify the normalization condition (2) and the electron continuity equation (40). The system convergence test is applied to the $f(r,u)$ solution and to the electron macroscopic equations (particle and power balance equations), checking for relative errors less than 10^{-6} and 10^{-10}, respectively.

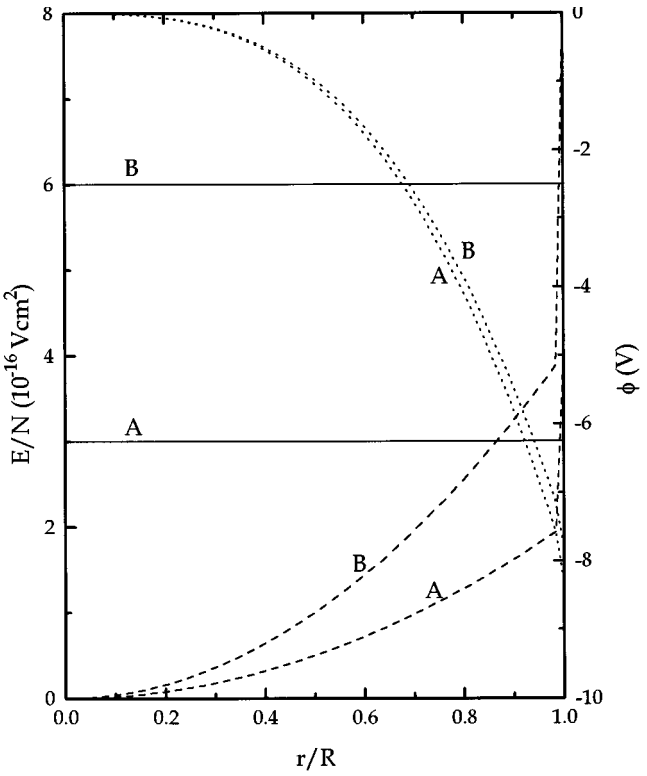

FIG. 5. Radial profiles for the reduced fields and the space-charge potential as a function of r/R, for the following work conditions: *A*, $E_z/N=3\times10^{-16}$ V cm^2 and $NR=1.2\times10^{17}$ cm^{-2}; and *B*, $E_z/N=6\times10^{-16}$ V cm^2 and $NR=5.5\times10^{16}$ cm^{-2}. The space-charge field E_r was calculated using Eq. (45). Solid curves, for the reduced maintaining field E_z/N; dashed curves, for the reduced space-charge field E_r/N; dotted curves, for the space-charge potential ϕ.

VII. SPACE-CHARGE FIELD. TOTAL ENERGY FORMULATION

In principle, the space-charge field $E_r(r)$ and the potential drop $\Delta\phi$ can be self-consistently determined by coupling the EBE with fluid-type equations for the ions, and Poisson's equation. However, in this work, these quantities are imposed as external parameters, but their influence on the final results is carefully analyzed.

By performing extensive numerical simulations, we have concluded that a physical solution to the problem requires the fulfillment of the following conditions.

(i) Near the axis, the space-charge field must *increase slowly* from zero, in order that the radial drift velocity be always directed toward the wall; for example, a linear-type law for $E_r(r)$, like the one used in [20], is not suitable for this purpose.

(ii) Near the wall, the space-charge field must present a *strong increase*, in order to limit the electron diffusion losses.

(iii) The magnitude of the potential drop $\Delta\phi$ must be such that it yields the *correct electron flux* at the tube wall, $\Gamma_r(r=R)$. In fact, the magnitude of the electron flux is very sensitive to the variations in the potential drop, in such a way that Γ_r decreases when $\Delta\phi$ increases.

In view of this, we have assumed a cubic-type law for ϕ, yielding a space-charge field with the general form

$$E_r(r)=\begin{cases} a\left(\dfrac{r}{R}\right)^2, & \text{if } 0\leqslant\dfrac{r}{R}\leqslant1-\dfrac{\Delta r}{R} \\ E_w\left(\dfrac{r}{R}\right)^2, & \text{if } 1-\dfrac{\Delta r}{R}\leqslant\dfrac{r}{R}\leqslant1, \end{cases} \tag{45}$$

where E_w is the space-charge field at the wall, a is a constant to be determined by continuity, and Δr is the discretization step along the radial direction. In Fig. 5 we present, for the corresponding *NR eigenvalues*, the radial profile of the reduced fields E_z/N and $E_r(r)/N$, and the radial profile of the potential $\phi(r)$ as adopted for the numerical simulations presented in this work.

With the space-charge field imposed here as an external parameter, we have not used a formulation in terms of the electron *total energy* (kinetic plus potential), since this would imply the use of an *arbitrary* potential distribution as an independent variable. This fact could, consequently, introduce important distortions in the description of all phenomena, even of those not directly dependent on the potential energy, like the collisional processes.

The *total energy formulation* has recently been used by various authors [20,21] to solve the spatially inhomogeneous EBE. The great advantage of this formulation lies in the fact that it formally transforms the EBE into a diffusionlike equation, allowing some convenient simplifications at low pressures, when collisional processes play a less important role in the discharge physics, (this is the main idea behind the so-called *nonlocal model* based on the works of Bernstein and Holstein [22] and Tsendin [23]). However, when dealing with the *general problem* of the nonlocal electron kinetics by solving the *complete EBE*, there are no special reasons justifying the use of the *total energy formulation*. On the contrary, it is our belief that this formulation *cannot provide a good physical description* in the strongly collisional domain of intermediate to high pressures here studied (cf. Sec. II B), unless a fully self-consistent resolution is carried out involving the Boltzmann equation for the electrons, the fluid-type equations for the ions, and Poisson's equation.

VIII. RESULTS AND DISCUSSION

The simulations presented in this work were made for helium, adopting the set of electron cross sections derived in [62,63]. We have used the field distributions represented in Fig. 5, corresponding to $E_z/N=3\times10^{-16}$ V cm^2, $NR=1.2\times10^{17}$ cm^{-2} and $E_z/N=6\times10^{-16}$ V cm^2, $NR=5.5\times10^{16}$ cm^{-2} (hereafter referred to as the *set of conditions I and II*, respectively), imposing $E_w/N\approx1.33E_z/N$ and $\Delta\phi=10$ V. Note that the *discharge characteristic* values $(E_z/N,\ NR)$ obtained with this model are shifted toward higher reduced applied fields as compared to the results in [64], due to the neglet of stepwise ionization processes in the present model.

Figures 6(a) and 6(b) represent, for conditions I and II, respectively, the isotropic component of the EDF $f(r,u)$, as a function of u for different radial positions $(r/R=0;0.5;1)$, together with the $f(u)$ distribution for the

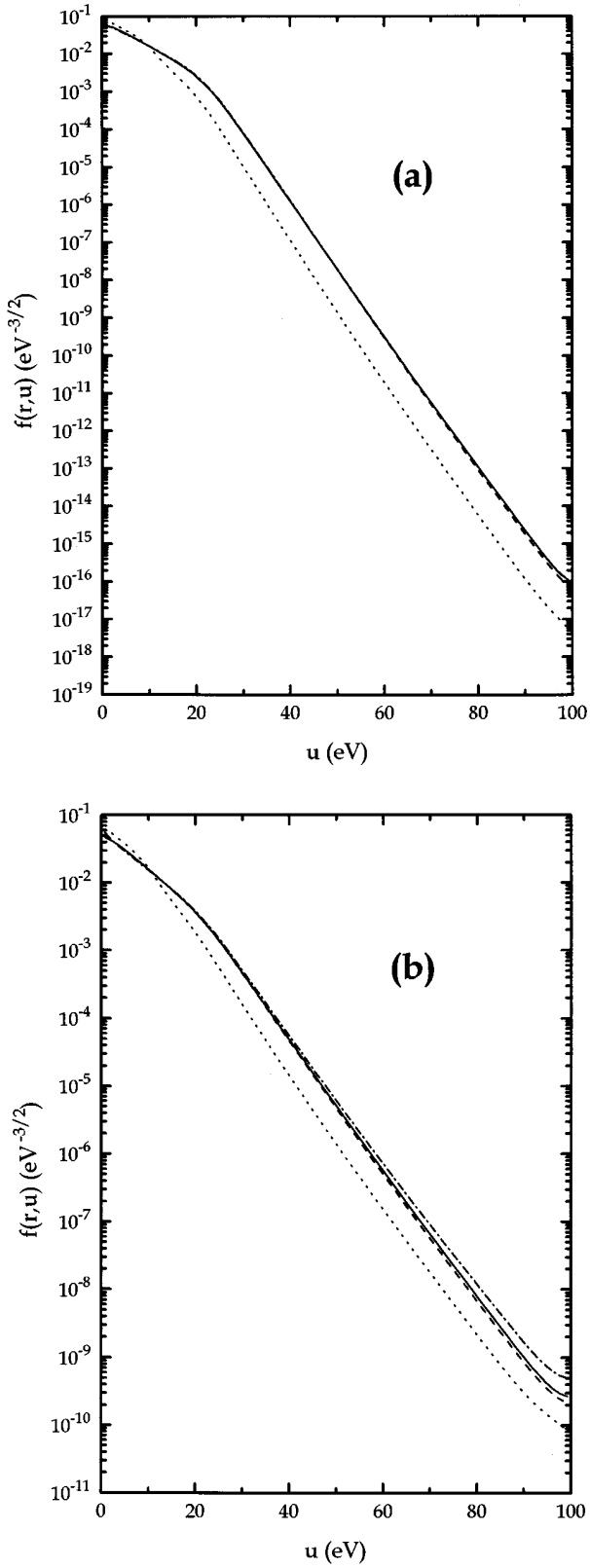

FIG. 6. Isotropic component of the EDF as a function of u, (a) for $E_z/N=3\times10^{-16}$ V cm^2 and $NR=1.2\times10^{17}$ cm^{-2}, and (b) for $E_z/N=6\times10^{-16}$ V cm^2 and $NR=5.5\times10^{16}$ cm^{-2}. The calculations were made assuming $\Delta\phi=10$ V, and E_r as given by Eq. (45). Solutions to the inhomogeneous EBE at the following r/R positions: solid curve, 0; dashed curve, 0.5; dotted curve, 1. The dash-dotted curve is for the solution to the homogeneous EBE. Each curve was renormalized to 1, that is, $\int_0^\infty f(r,u)\sqrt{u}du=1$.

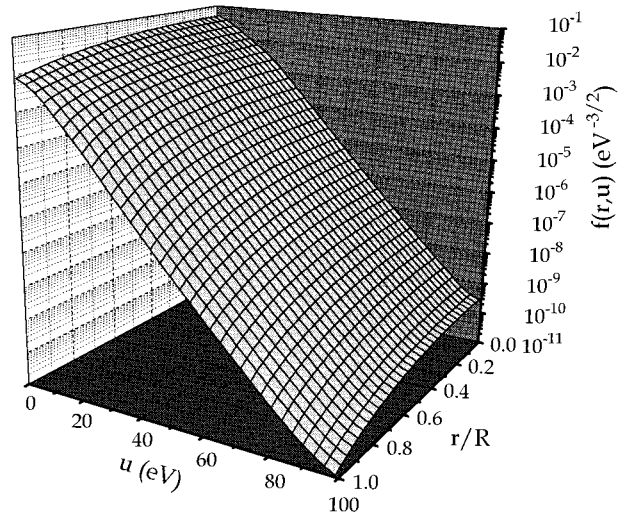

FIG. 7. Isotropic component of the EDF as a function of r/R and u, for $E_z/N=6\times10^{-16}$ V cm^2, $NR=5.5\times10^{16}$ cm^{-2}, $\Delta\phi=10$ V, and E_r as given by Eq. (45).

corresponding homogeneous situation. For purposes of comparison, each function was renormalized to 1, that is, $\int_0^\infty f(r,u)\sqrt{u}du=1$. A 3D plot of $f(r,u)$ vs $(r/R,u)$ is also represented in Fig. 7 for condition II. These figures clearly show the depletion of the isotropic EDF as the boundary at $r=R$ is approached, due to the electron drain to the wall. The distribution at the axis is closer to the homogeneous solution, but the deviations become stronger as E_z/N increases, which is indicative of an enhanced nonlocal behavior.

The radial electron density distribution $n_e(r)/n_0$ is represented in Fig. 8 as a function of r/R, for the set of conditions I and II. For comparison, we have also plotted in this figure the density distributions assuming a Boltzmann equilibrium with the space-charge field, $n_e(r)/n_0=\exp(\phi(r)/T_e)$ (T_e is the radially averaged electron temperature with $T_e\equiv(2/3)\langle u\rangle$), and the typical Bessel distribution with $n_e(R)=0$.

The electron ionization rate coefficient ν_I/N [cf. Eq. (37)], the electron characteristic energy $u_k=D/\mu$ [cf. Eqs. (39a) and (39b)], and the mean power absorbed from the applied field per electron at unit gas density Θ/N [cf. Eq. (43)], are shown in Figs. 9, 10, and 11, respectively, as a function of r/R and for the set of conditions I and II. In each of these figures, we also represent the data calculated for the homogeneous situation. We observe that the values of these quantities across the discharge, calculated using the spatially dependent EDF, are always below those corresponding to the homogeneous situation, due to the loss of electrons to the wall. As expected, this nonlocal effect becomes more important as the reduced applied field increases.

Figures 12(a) and 12(b) represent, for condition I, the isotropic component of the EDF $f(r,u)$, and the anisotropic components, $f_z^1(r,u)$ and $f_r^1(r,u)$, as a function of u for different radial positions: $r/R=0.5;1$. These figures show that the axial anisotropy is *always directed against the reduced applied field* E_z/N ($\partial f(r,u)/\partial u<0$) [cf. Eq. (3b)], while the radial anisotropy *normally points toward the wall* ($|\nabla_r f(r,u)|>E_r(r)|\partial f(r,u)/\partial u|$) [cf. Eq. (3c)], which means that the *electrons do flow toward the wall against the*

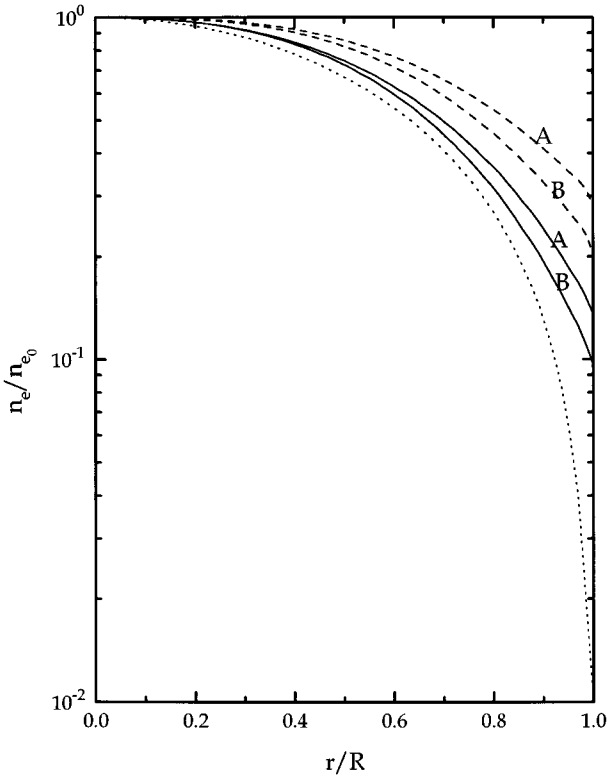

FIG. 8. Electron density radial distribution as a function of r/R, for the following work conditions: A, $E_z/N=3\times10^{-16}$ V cm^2 and $NR=1.2\times10^{17}$ cm^{-2}; and B, $E_z/N=6\times10^{-16}$ V cm^2 and $NR=5.5\times10^{16}$ cm^{-2}. The calculations were made assuming $\Delta\phi=10$ V, and E_r as given by Eq. (45). Solid curves: solutions to the inhomogeneous EBE. Dashed curves: calculations assuming a Boltzmann equilibrium with the space-charge field, i.e., $n_e(r)/n_{e_0}=\exp(\phi(r)/\overline{T_e})$, where $\overline{T_e}$ is the radially averaged electron temperature. Dotted curves: Bessel distribution taking $n_e(R)=0$.

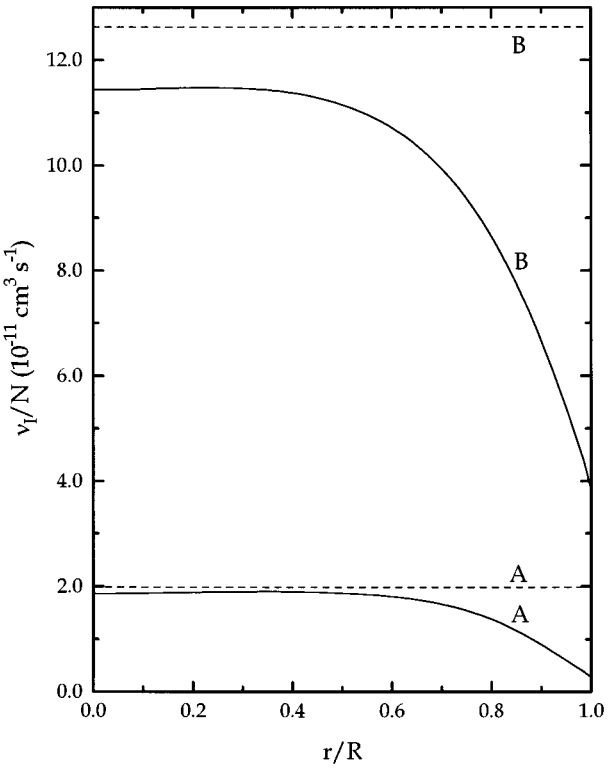

FIG. 9. Electron ionization rate coefficient as a function of r/R, for the following work conditions: A, $E_z/N=3\times10^{-16}$ V cm^2 and $NR=1.2\times10^{17}$ cm^{-2}; and B, $E_z/N=6\times10^{-16}$ V cm^2 and $NR=5.5\times10^{16}$ cm^{-2}. The calculations were made assuming $\Delta\phi=10$ V, and E_r as given by Eq. (45). Solid curves: solutions to the inhomogeneous EBE. Dashed curves: solutions to the homogeneous EBE.

space-charge field. However, an exception to this occurs for an intermediate range of the kinetic energy, where f_r^1 becomes negative. To understand this behavior we must go back to Eq. (3c) for the radial anisotropy, which can be rewritten as

$$f_r^1=\frac{1}{N\sigma_t}\left[E_r\frac{\partial f}{\partial u}-\nabla_r f\right]=\frac{1}{N\sigma_t}\left|\frac{d\phi}{dr}\right|\left[-\left|\frac{\partial f}{\partial u}\right|+\left|\frac{\partial f}{\partial \phi}\right|\right]. \tag{46}$$

Equation (46) interprets the formation of f_r^1 as the result of a balance between the variations of f with the kinetic energy u and the potential energy ϕ. In this way, f_r^1 is negative whenever the term $|\partial f/\partial u|$ dominates over $|\partial f/\partial\phi|$. This happens in a region of intermediate kinetic energies, beyond an energy around the inelastic thresholds, where the excitations and ionizations strongly deplete the electron energy distribution.

Two further remarks are required to fully understand this question. First, as we can see from Fig. 12(b), the radial anisotropy *always points toward the wall* at $r=R$, due to the strong electron drain occurring in this region. This is a direct consequence of the wall boundary condition deduced here, which yields a vanishing radial anisotropy if the electron kinetic energy along r, $u_\perp$, is smaller than the potential drop $\Delta\phi$, and a forward directed radial anisotropy otherwise [cf. Eqs. (14), (21a), and (22)]. Second, in view of the above considerations we can expect to have a strong correlation between the behavior in sign of f_r^1 and the reduced applied field strength. Figures 13(a) and 13(b) represent a contour plot of $f_r^1(r,u)$ vs $(r/R,u)$ for the set of conditions I, and for $E_z/N=1.5\times10^{-16}$ V cm^2 and $NR=3.1\times10^{17}$ cm^{-2}, respectively. From these figures we observe that, when E_z/N decreases, there is a broadening (both in r and u) of the region where f is strongly influenced by the excitations and ionizations, and f_r^1 is negative. In fact, for $E_z/N=3\times10^{-16}$ V cm^2, this region starts at $u\approx25$ eV, where a *collisional barrier* develops, reaching the maximum values of $u\approx80$ eV and $r/R\approx0.8$, whereas for $E_z/N=1.5\times10^{-16}$ V cm^2 the starting zone drops to $u\approx20$ eV and the maximum values attained move to $u\gtrsim100$ eV and $r/R\approx0.95$.

The low field situation represented in Fig. 13(b) reproduces in part the results of Urhlandt and Winkler [21], whose numerical simulations yield a radial anisotropy pointing to the wall for the lower kinetic energies, and to the axis for the higher ones, regardless of the spatial position. We do disagree, however, with the observations of these authors, as they seem to infer that f_r^1 is always negative, even near the wall, at high kinetic energies. This conclusion comes out as a result of their semi-empirical wall boundary condition, combined with a restricted analysis based only on low E_z/N

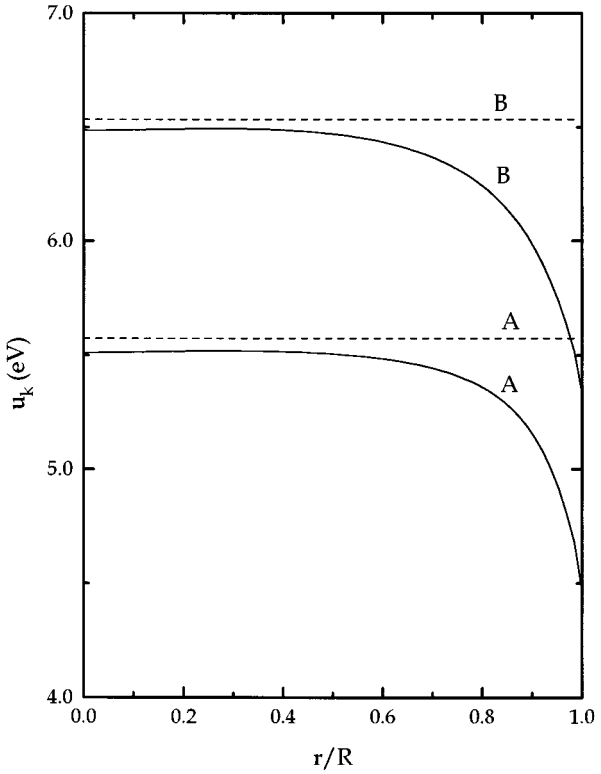

FIG. 10. Electron characteristic energy as a function of r/R, for the following work conditions: *A*, $E_z/N=3\times10^{-16}$ V cm^2 and $NR=1.2\times10^{17}$ cm^{-2}; and *B*, $E_z/N=6\times10^{-16}$ V cm^2 and $NR=5.5\times10^{16}$ cm^{-2}. The calculations were made assuming $\Delta\phi=10$ V, and E_r as given by Eq. (45). Solid curves: solutions to the inhomogeneous EBE. Dashed curves: solutions to the homogeneous EBE.

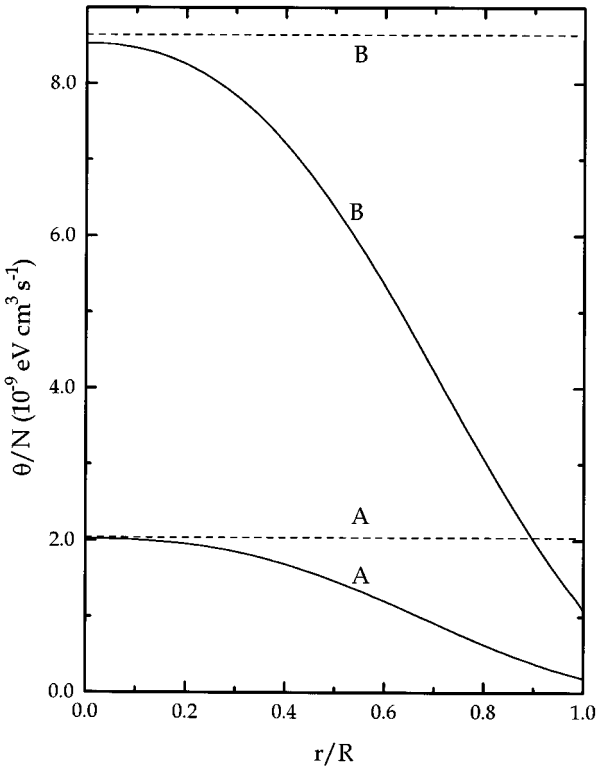

FIG. 11. Mean power absorbed from the applied field per electron at unit gas density as a function of r/R, for the following work conditions: *A*, $E_z/N=3\times10^{-16}$ V cm^2 and $NR=1.2\times10^{17}$ cm^{-2}; and *B*, $E_z/N=6\times10^{-16}$ V cm^2 and $NR=5.5\times10^{16}$ cm^{-2}. The calculations were made assuming $\Delta\phi=10$ V, and E_r as given by Eq. (45). Solid curves: solutions to the inhomogeneous EBE. Dashed curves: solutions to the homogeneous EBE.

values. As a matter of fact, the change in sign of f_r^1 is by no means a general feature for all E_z/N values; numerical tests showed that for $E_z/N\gtrsim4\times10^{-16}$ V cm^2 this effect no longer occurs, as the electrons are sufficiently accelerated by the applied field to cross the *collisional barrier* without being significantly affected by it.

The strong variation of f with u, beyond the *collisional barrier* around the inelastic thresholds, is also responsible for the fact that $|f_z^1|\simeq f$ from $u\gtrsim20$ eV. This observation agrees with the results obtained by Pitchford, O'Neil, and Rumble [14], who analyzed the corrections introduced in the macroscopic coefficients when more than two terms are retained in the Legendre expansion (1a) of the EDF. A consequence of this fact was previously reported [62] while deducing a cross section set for direct excitations and ionization in helium, by fitting the Townsend ionization coefficient. In both works the conclusion is that a multiterm expansion is required whenever high accuracy results are requested.

A similar problem occurs with the radial anisotropy at $r=R$, where $f_r^1\simeq f$ for $u\gtrsim25$ eV [see Fig. 12(b)]. This violation of the two-term approximation is a direct result of the wall boundary condition [cf. Eqs. (21a) and (22)], as $\xi(u,\Delta\phi=10\text{ V})\gtrsim1$ for $u\gtrsim25$ eV.

The radial drift velocity v_d can be obtained from the radial anisotropy using Eq. (26b). In Fig. 14 we represent v_d vs r/R for the set of conditions II, assuming the potential drops $\Delta\phi=4$ V and 10 V. The unphysical decrease of v_d near the wall for $\Delta\phi=10$ V shows that this potential drop is high enough to slow down the electron flux across the *boundary layer*; in that sense, $\Delta\phi=4$ V is a more realistic value for the potential drop. As noted before (Sec. VII), a self-consistent determination of $\Delta\phi$ requires the inclusion of the ion kinetics in order to equate the electron and the ion fluxes at the wall.

The distribution of the fractional power lost by the electrons is shown in Fig. 15 as a function of r/R, for the set of conditions I and II. The curves plotted here correspond to the different terms of the electron power balance equation [cf. Eqs. (41)–(44e)]: the fractional power lost by the electrons due to the radial transport in the discharge, $\Theta_{\text{transp}}/\Theta$, in elastic collisions, P_{el}/Θ, in excitations, P_{exc}/Θ, and in ionizations, P_{ion}/Θ. As expected, the main electron power loss channel is associated with excitation collisions, throughout most of the discharge cross section, to become mainly due to the radial transport of the electrons, near the wall.

The two components of $\Theta_{\text{transp}}/\Theta$ can be unfolded into the power lost by the electrons in flowing against the space-charge field, P_{E_r}, and that due to the radial flux in configuration space, P_{conv}. Figure 16 represents $\Theta/(\Theta-P_{\text{conv}})$, $-P_{E_r}/(\Theta-P_{\text{conv}})$, and $-P_{\text{conv}}/(\Theta-P_{\text{conv}})$ as a function of r/R, for the set of conditions I and II. Note that the positive (negative) values in this figure indicate an electron power gain (loss). Further note that the percentages are now calculated relative to the *net power gain*, $\Theta-P_{\text{conv}}$, because the

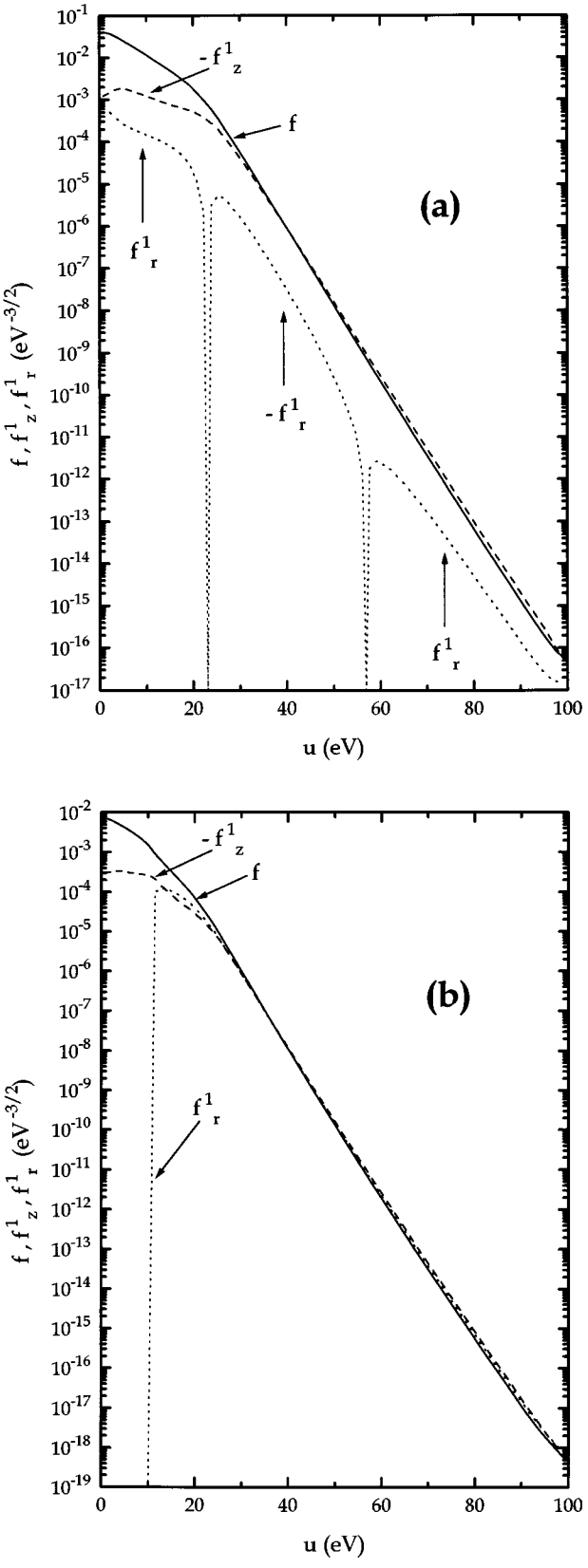

FIG. 12. Isotropic and anisotropic components of the EDF as a function of u, for $E_z/N = 3\times10^{-16}$ V cm^2, $NR = 1.2\times10^{17}$ cm^{-2}, $\Delta\phi = 10$ V, and E_r as given by Eq. (45), at the following r/R positions: (a) 0.5 and (b) 1. Solid curves: isotropic component f. Dashed curves: axial anisotropic component $|f_z^1|$. Dotted curves: radial anisotropic component $|f_r^1|$.

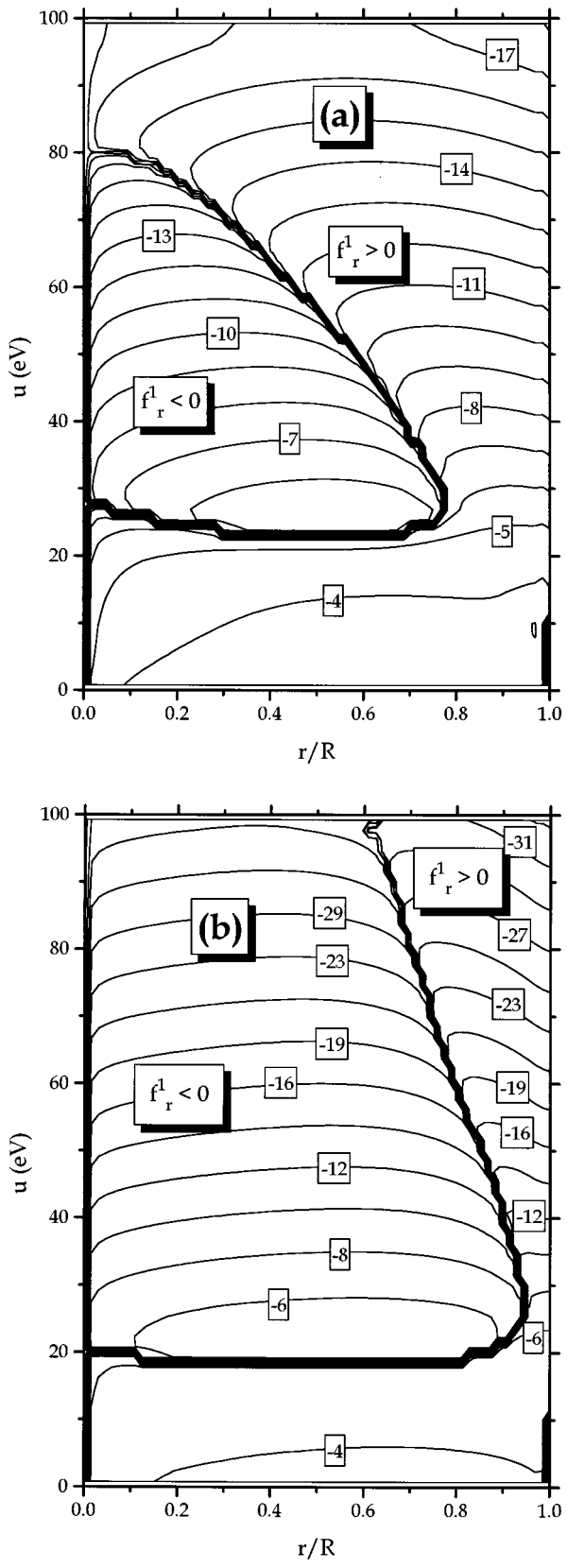

FIG. 13. Countour plot of $\log_{10}|f_r^1|$ as a function of r/R and u, (a) for $E_z/N = 3\times10^{-16}$ V cm^2 and $NR = 1.2\times10^{17}$ cm^{-2}, and (b) for $E_z/N = 1.5\times10^{-16}$ V cm^2 and $NR = 3.1\times10^{17}$ cm^{-2}. The calculations were made assuming $\Delta\phi = 10$ V, and E_r as given by Eq. (45).

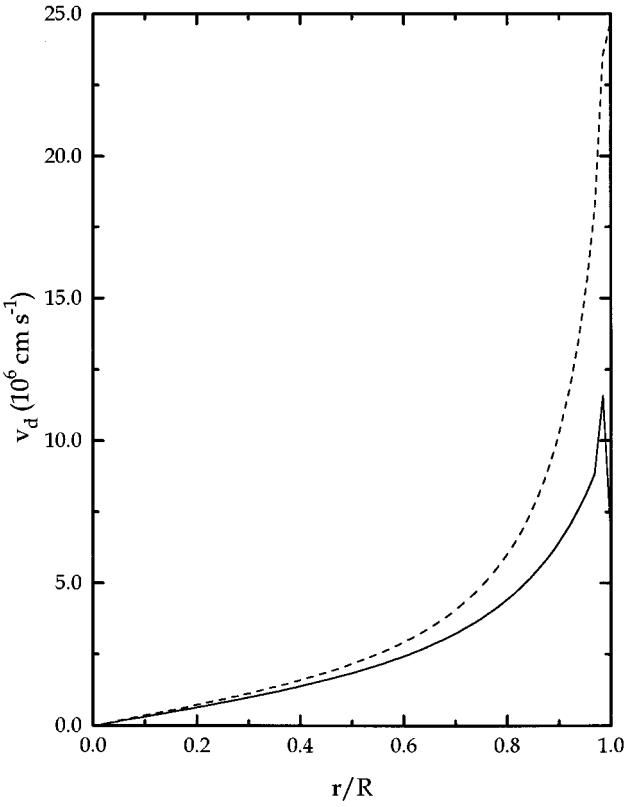

FIG. 14. Electron radial drift velocity as a function of r/R, for $E_z/N=6\times10^{-16}$ V cm^2, $NR=5.5\times10^{16}$ cm^{-2}, E_r as given by Eq. (45), and the following potential drops $\Delta\phi$: solid curve, 10 V; dashed curve, 4 V.

quantity P_{conv} can represent either a loss or a gain of power [depending on whether the divergence in Eq. (44b) is positive or negative, respectively]. As seen from Fig. 16, the term $-P_{\text{conv}}$ becomes positive close to the wall, which means that the divergence of the power flow by convection is negative. Physically, this corresponds to a gain of power in this region due to heat convection. Such a gain is necessary to overcome the increased losses associated with the rapid increase in the space-charge field near the wall (note that $P_{E_r}\gtrsim|P_{\text{conv}}|$ near the wall). These results agree, in general, with the ones presented by Uhrlandt and Winkler [21].

IX. CONCLUDING REMARKS

In this paper we developed a *self-contained formulation* to solve the steady-state spatially inhomogeneous EBE numerically, including the spatial gradient and the space-charge field terms, using the classical *two-term approximation*. The problem was solved for a dc positive column in He of radius R, under the action of a total electric field of the form $\vec{E}(r)=E_r(r)\vec{e}_r+E_z\vec{e}_z$, where the radial component $E_r(r)=-\nabla_r\phi$ is the space-charge field (ϕ represents the space-charge potential), and the axial one is the applied electric field, assumed to be uniform. Our study was focused on the electron kinetics, so a cubic-type law was assumed for the radial profile of ϕ.

We carried out a detailed discussion to deduce the appropriate boundary conditions for the electron velocity distribution function, both in configuration and in energy spaces. Special attention was given to the wall region, where we defined an infinitely thin *boundary layer* with a potential drop $\Delta\phi$; at the entrance of this layer, we imposed a boundary condition expressing that the microscopic radial flux of electrons, as obtained from f_r^1, exactly matches the flux of electrons with sufficient kinetic energy along r to overcome the potential drop $\Delta\phi$. This yields $f_r^1(R,u)=\xi(u)f(R,u)$, where $\xi(u)$ is calculated by considering a *loss cone to the wall*; the validity of this condition was tested by considering various well-known limiting situations.

We adopted a *kinetic energy formulation*, in opposition to the *total energy formulation* recently used by other authors [20,21], to work out solutions to the complete spatially inhomogeneous EBE. In fact, because we are considering the space-charge field as an external parameter, a formulation in terms of the electron *total energy* (kinetic plus potential) would imply the use of an arbitrary potential distribution as an independent variable. Consequently, some important distortions could be introduced in the description of all phenomena, even of those not directly dependent on the potential energy, like the collisional processes, especially in the range of intermediate to high pressures here studied.

Further, the formulation developed in this paper is *self-contained* in the sense that the electron particle balance equation is verified. This requires an ionization rate that exactly compensates for the electron loss rate to the wall. This condition yields the relationship between the applied reduced maintaining field E_z/N, and the product NR, termed the *discharge characteristic*, which was simultaneously obtained as an *eigenvalue solution* to the problem. Such a formulation constitutes the sole correct approach for consistently solving this nonlocal kinetic problem, as it does not resort to experimental *discharge characteristics* as input data [20,21].

The system formed by the EBE and the appropriate normalization condition for the EDF was solved using a powerful *multigrid method*, conveniently modified to treat mixed, i.e., Dirichlet and Neumann, boundary conditions together with *eigenvalue* calculations. We obtained the isotropic and anisotropic components of the EDF, from which we deduced the radial distributions of all relevant macroscopic quantities: electron density, electron transport parameters and rate coefficients for excitation and ionization, and electron power transfer. These radial distributions were shown to be below the values calculated for a homogeneous situation, due to the loss of electrons to the wall. As expected, this nonlocal effect becomes more important as the reduced applied field increases.

The solutions obtained for the EDF revealed that, for sufficiently low maintaining fields, $E_z/N\lesssim4\times10^{-16}$ V cm^2, the radial anisotropy presents negative values in a bounded energy region, above a *collisional barrier* around the inelastic thresholds, in which this anisotropy is directed toward the discharge axis; however, at the wall, the radial anisotropy always points to the wall, due to the strong electron drain occurring in this region. The general analysis presented here, concerning the radial anisotropy, clarifies the physical behavior of f_r^1 previously reported by other authors [21]. In all cases, however, the electron drift velocity points to the wall, meaning that we can characterize the radial electron transport in the discharge as a *diffusion-controlled regime*, in which

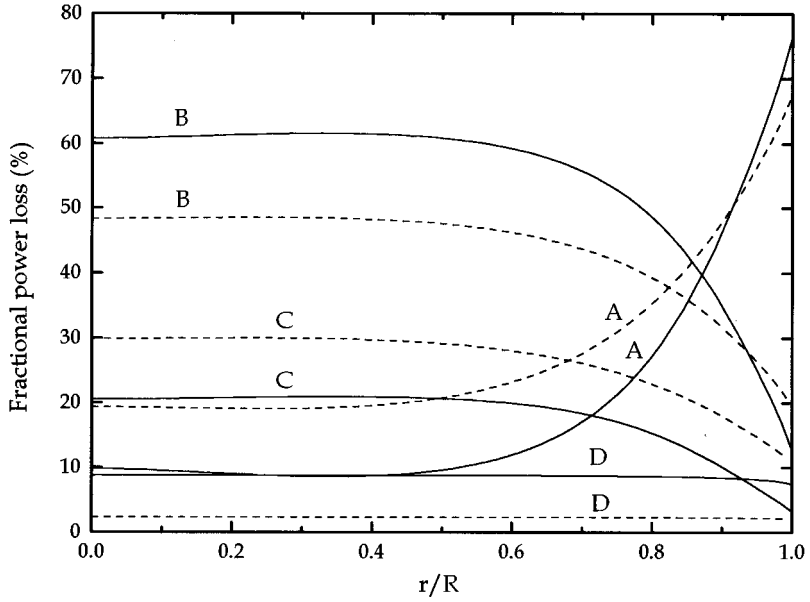

FIG. 15. Average fractional power lost by the electrons vs r/R, for the following work conditions: solid curves, $E_z/N=3\times10^{-16}$ V cm^2 and $NR=1.2\times10^{17}$ cm^{-2}; dashed curves, $E_z/N=6\times10^{-16}$ V cm^2 and $NR=5.5\times10^{16}$ cm^{-2}. The calculations were made assuming $\Delta\phi=10$ V, and E_r as given by Eq. (45). The labels correspond to the following power loss channels: *A*, radial transport in the discharge (diffusion against the space-charge field + convection flow in configuration space); *B*, inelastic excitations; *C*, ionizations; and *D*, elastic collisions.

the electrons do flow toward the wall against the space-charge field and the friction force due to collisions.

Further, we observed that $|f_z^1|\simeq f$ for $u\gtrsim20$ eV, irrespectively of the discharge position, and that $f_r^1\simeq f$ for $u\gtrsim25$ eV at $r=R$. These results show that, for our conditions, the validity of the *two-term approximation* fails, so that a multiterm expansion is required for higher accuracy [14].

We also analyzed the fractional power transfer distribution in the discharge, to conclude that the main electron power loss channel is associated with the inelastic excitations, throughout most of the discharge cross section. However, near the wall, the power flow due to the radial transport of electrons becomes predominant. In this region, the enhanced power losses associated with the rapid increase of the space-charge field are balanced by a gain of power due to heat convection.

The present model gives a *self-contained* description of the nonlocal electron kinetics, for a range of intermediate to high pressures, allowing the characterization of a dc positive column in terms of the radial transport and the power transfer distribution. The complete resolution of this nonlocal kinetic problem still requires, however, the determination of the space-charge potential and the potential drop $\Delta\phi$ in a *self-consistent* way, by coupling the Boltzmann equation for the electrons with the fluid-type equations for the ions, and Poisson's equation. Work is in progress in this direction.

ACKNOWLEDGMENTS

The authors wish to thank Dr. U. Kortshagen and C. Busch for many exchanges of ideas. This work was supported by *PRAXIS XXI* Programme and FEDER uner Contract No. Fis/377/94. One of us (L.L.A.) received financial support from *PRAXIS XXI* Programme to carry part of this work at the University Paris XI, Orsay.

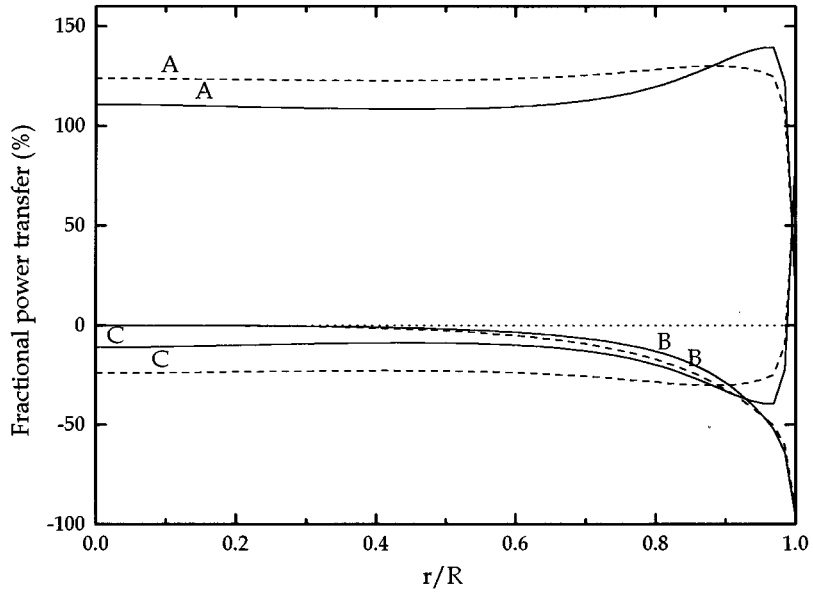

FIG. 16. Average fractional power gained/lost by the electrons vs r/R, for the following work conditions: solid curves, $E_z/N=3\times10^{-16}$ V cm^2 and $NR=1.2\times10^{17}$ cm^{-2}; dashed curves, $E_z/N=6\times10^{-16}$ V cm^2 and $NR=5.5\times10^{16}$ cm^{-2}. The dotted line corresponds to a zero-power transfer. The calculations were made assuming $\Delta\phi=10$ V, and E_r as given by Eq. (45). The labels correspond to the following power transfer channels: *A*, acceleration by the applied field; *B*, diffusion against the space-charge field; and *C*, convection flow in configuration space. The positive (negative) values indicate a power gain (loss) by the electrons. Percentages were calculated relative to the net power gain from the $A+C$ mechanisms.

[1] M. Surendra and D. B. Graves, IEEE Trans. Plasma Sci. **19**, 144 (1991).
[2] T. J. Sommerer and M. J. Kushner, J. Appl. Phys. **71**, 1654 (1992).
[3] W. N. G. Hitchon, G. J. Parker, and J. E. Lawler, IEEE Trans. Plasma Sci. **21**, 228 (1993).
[4] V. Vahedi *et al.*, Phys. Fluids B **5**, 2719 (1993).
[5] V. Vahedi *et al.*, Plasma Sources Sci. Technol. **2**, 261 (1993).
[6] P. L. G. Ventzek, T. J. Sommerer, R. J. Hoekstra, and M. J. Kushner, Appl. Phys. Lett. **63**, 605 (1993).
[7] P. L. G. Ventzek, R. J. Hoekstra, and M. J. Kushner, J. Vac. Sci. Technol. B **12**, 461 (1994).
[8] M. J. Kushner, J. Appl. Phys. **54**, 4958 (1983).
[9] H. N. G. Hitchon, D. J. Koch, and J. B. Adams, J. Comput. Phys. **83**, 79 (1989).
[10] T. J. Sommerer, W. N. G. Hitchon, and J. E. Lawler, Phys. Rev. A **39**, 6356 (1989).
[11] G. J. Parker, W. N. G. Hitchon, and J. E. Lawler, Phys. Rev. E **50**, 3210 (1994).
[12] T. Holstein, Phys. Rev. **70**, 367 (1946).
[13] W. P. Allis, in *Handbuch der Physik*, edited by S. Flügge (Springer, Berlin, 1956), Vol. 21, p. 383.
[14] L. C. Pitchford, S. V. O'Neil, and J. R. Jr. Rumble, Phys. Rev. A **23**, 294 (1981).
[15] R. Winkler, H. Deutsch, J. Wilhelm, and Ch. Wilke, Beitr. Plasmaphys. **24**, 285 (1984).
[16] V. A. Feoktistov *et al.*, IEEE Trans. Plasma Sci. **19**, 163 (1991).
[17] P. M. Meijer, W. J. Goedheer, and J. D. P. Passchier, Phys. Rev. A **45**, 1098 (1992).
[18] M. J. Hartig and M. J. Kushner, J. Appl. Phys. **73**, 1080 (1993).
[19] F. Sigeneger and R. Winkler, Phys. Rev. E **52**, 3281 (1995).
[20] C. Busch and U. Kortshagen, Phys. Rev. E **51**, 280 (1995).
[21] D. Uhrlandt and R. Winkler, J. Phys. D **29**, 115 (1996).
[22] I. B. Bernstein and T. Holstein, Phys. Rev. **94**, 1475 (1954).
[23] L. D. Tsendin, Zh. Éksp. Teor. Fiz. **66**, 1638 (1974) [Sov. Phys. JETP **39**, 805 (1974)].
[24] L. D. Tsendin and Yu. B. Golubovskii, Zh. Tekh. Fiz. **47**, 1839 (1977) [Sov. Phys. Tech. Phys. **22**, 1066 (1977)].
[25] L. D. Tsendin, Zh. Tekh. Fiz. **56**, 278 (1986) [Sov. Phys. Tech. Phys. **31**, 169 (1986)].
[26] V. I. Kolobov and L. D. Tsendin, Phys. Rev. A **46**, 7837 (1992).
[27] I. D. Kaganovich and L. D. Tsendin, IEEE Trans. Plasma Sci. **20**, 66 (1992).
[28] V. I. Kolobov, D. F. Beale, L. J. Mahoney, and A. E. Wendt, Appl. Phys. Lett. **65**, 537 (1994).
[29] U. Kortshagen and L. D. Tsendin, Appl. Phys. Lett. **65**, 1355 (1994).
[30] U. Kortshagen, I. Pukropski, and L. D. Tsendin, Phys. Rev. E **51**, 6063 (1995).
[31] V. I. Kolobov and W. N. G. Hitchon, Phys. Rev. E **52**, 972 (1995).
[32] U. Kortshagen, J. Phys. D **26**, 1691 (1993).
[33] L. L. Alves, C. M. Ferreira, C. Busch, and U. Kortshagen, in *Proceedings of the XXII International Conference of Phenomena on Ionized Gases*, edited by K. H. Becker, W. E. Carr, and E. E. Kunhardt (Stevens Institute of Technology, New York, 1995), Vol. 4, p. 217.
[34] V. E. Golant, A. P. Zhilinsky, and I. E. Sakharov, in *Fundamentals of Plasma Physics*, edited by S. C. Brown (Wiley, New York, 1980).
[35] M. Abramowitz and I. A. Stegun, *Handbook of Mathematical Functions* (Dover, New York, 1970).
[36] R. Balescu, *Equilibrium and Nonequilibrium Statistical Mechanics* (Wiley, New York, 1975).
[37] T. Y. Wu, *Kinetic Equation of Gases and Plasmas* (Addison-Wesley, Reading, MA, 1966), Chap. 2.
[38] E. Blue, J. H. Ingold, and W. J. Ozeroff, Phys. Fluids **5**, 1576 (1962).
[39] E. Blue and J. H. Ingold, Plasma Phys. **10**, 899 (1968).
[40] J. H. Ingold, Phys. Fluids **15**, 75 (1972).
[41] R. N. Franklin, *Plasma Phenomena in Gas Discharges* (Clarendon, Oxford, 1976).
[42] A. Metze, D. W. Ernie, and H. J. Oskam, Phys. Rev. A **39**, 4117 (1989).
[43] H.-B. Valentini, J. Phys. D **21**, 311 (1988).
[44] H.-B. Valentini, J. Phys. D **27**, 119 (1994).
[45] P. Morse and H. Feshbach, *Methods of Theoretical Physics* (McGraw-Hill, New York, 1953), Pt. I, p. 185.
[46] B. Davison and J. B. Sykes, *Neutron Transport Theory* (Clarendon, Oxford, 1958), Chap. VI, VIII, and X.
[47] A. Schuster, Astrophys. J. **21**, 1 (1905).
[48] K. Schwarzschild, Phys. Tech. **17**, 1183 (1914).
[49] G. C. Wick, Z. Phys. **120**, 702 (1943).
[50] S. Chandrasekhar, *Radiative Transfer* (Clarendon, Oxford, 1950).
[51] W. Shockley, Phys. Rev. **125**, 1570 (1962).
[52] P. J. Chantry, A. V. Phelps, and G. Schulz, Phys. Rev. **152**, 81 (1966).
[53] A. V. Phelps, J. Res. Natl. Inst. Stand. Technol. **95**, 407 (1990).
[54] P. J. Chantry, J. Appl. Phys. **62**, 1141 (1987).
[55] W. Schottky, Phys. Z. **25**, 635 (1924).
[56] W. P. Allis and D. J. Rose, Phys. Rev. **93**, 84 (1954).
[57] S. D. Rockwood, Phys. Rev. A **8**, 2348 (1973).
[58] C. J. Elliott and A. E. Greene, J. Appl. Phys. **47**, 2946 (1976).
[59] W. Hackbush, *Multi-Grid Methods and Applications* (Springer-Verlag, Berlin, 1985).
[60] W. H. Press, B. P. Flannery, S. A. Teukolsky, and W. T. Vetterling, *Numerical Recipes. The Art of Scientific Computing* (Cambridge University Press, Cambridge, 1992), p. 862.
[61] C. A. J. Fletcher, *Computational Techniques for Fluids Dynamics* (Springer-Verlag, New York, 1991), Vol. I, p. 203.
[62] L. L. Alves and C. M. Ferreira, J. Phys. D **24**, 581 (1991).
[63] G. D. Alkhazov, Zh. Tekh. Fiz. **40**, 97 (1970) [Sov. Phys. Tech. Phys. **15**, 66 (1970)].
[64] L. L. Alves, G. Gousset, and C. M. Ferreira, J. Phys. D **25**, 1713 (1992).